

# Fine-Scale Phenology of Urban Trees From Satellite Image Time Series: Toward a Comprehensive Analysis of Influencing Factors

Clément Bressant<sup>1</sup>, Pierre-Alexis Herrault<sup>1</sup>, and Anne Puissant<sup>1</sup>

**Abstract**—While satellite time series are essential tools to derive phenometrics at unprecedented spatial and temporal scales, non-systematic acquisition or medium spatial resolution of available missions is potentially problematic. At the same time, low-cost observation networks bridge the gap between satellite and in situ observations, which considerably increases ground-based data and associated possibilities. Here, we provide robust statistics about the reliability of satellite-derived phenometrics of urban trees across phenophases. Environmental and acquisition factors influencing the quality of phenometric estimates were analyzed. First, a multifacet regression-based analysis was conducted to measure discrepancies between PlanetScope (and Sentinel-2) and ground-based measurements across phenophases. Second, we performed hierarchical partitioning to tackle the effects of biological parameters (canopy closure and color leaf) for assessing phenometrics with satellite time series. Third, we ran Monte Carlo simulations to propagate errors according to viewing angles in PlanetScope acquisition. Our results show that: 1) PlanetScope provides consistent phenometric estimates for different tree layouts belonging to the same species (average  $R^2 = 0.50 \pm 0.18$ ); performances are higher than those of Sentinel-2 but duration-based phenometrics estimates were poorly reconstructed with both satellite missions; 2) contributions of biological parameters in the vegetation signal above trees strongly vary between growth periods; while canopy closure drives the growing season signal (independent contribution  $> 40\%$ ), color leaf plays a major role in the senescence season; and 3) variable viewing angles in PlanetScope acquisitions showed only significant effects on duration-based metrics estimates. Our research opens new perspectives for monitoring urban trees, which improves the measurement of ecosystem services for local inhabitants.

**Index Terms**—Discrepancies, high spatial resolution, phenology, PlanetScope (PS), satellite image time series (SITS), Sentinel-2 (S2), urban trees.

## I. INTRODUCTION

ORIGINALLY, urban trees were intended to enhance the visual aesthetics of highly urbanized areas [1]. Today, numerous additional benefits known as ecosystem services are assigned to these trees [2], [3]. Urban trees provide multiple ecosystem services, such as urban heat island mitigation [4], rainfall runoff reduction [5], carbon storage [6], shading [7],

and pollutant filtration [8]. They also offer specific ecological habitats for a large diversity of species, which, in turn, affects diverse city components [9]. Consequently, urban greening remains an effective local strategy for facing climate change and acts as an inhibitor of ongoing urbanization [10], [11]. Urban tree planting initiatives are one of the massive results of these local strategies and are largely encouraged by city councils, leading to an increase in the green fraction and green belts in cities worldwide [12], [13].

The measurements of ecosystem services offered by urban trees are closely related to tree characteristics, such as species, morphology, and age [14], [15]. For example, old trees, although very fragile and declining [16], [17], and often considered dangerous [18], have shown themselves to be important supports for biodiversity: habitat for fauna and flora and numerous other ecosystem processes due, in particular, to the extensive foliage and the organic matter it produces even in urban environment [19], [20]. These parameters are also strongly dependent on seasonality since photoperiods combined with seasonal climatic variations influence the composition and functioning of urban trees [21], [22]. In this context, phenology that features the timing of growth events and productivity measurements are essential since they allow for the monitoring of tree growth across seasons [23], [24].

Phenological and productivity-based surveys rely on various techniques and methods developed in recent decades [25]. Ground-based human observations allow the accurate identification of periods and durations [26]. Various methods, such as leaf budding, flowering, or leaf color change, are commonly used to directly observe and record phenological events based on organic development by researchers and/or management and conservation specialists. This involves visual assessments, photography, or manual data collection at specific locations within the trees. International and local networks, such as the European PEP725 network and/or the French SOERE TEMPO database, exist for monitoring and sharing these data at a large scale [27], [28]. However, for logistical and human reasons, these techniques are spatially and temporally limited. This approach results in few individuals being recorded at the city scale and in temporally incomplete datasets that bias the calculation of specific phenological estimates. Finally, the subjectivity and representation of the observations make these data difficult to integrate into spatial databases to establish connections between different types of measurements [29].

Optical remote sensing (RS) is an effective approach for ensuring the phenological monitoring of urban trees at

Manuscript received 30 December 2023; revised 21 April 2024 and 30 May 2024; accepted 2 June 2024. Date of publication 7 June 2024; date of current version 1 July 2024. This work was supported in part by the Grand-Est Region and in part by the University of Strasbourg under Grant ED413. (Corresponding author: Clément Bressant.)

The authors are with the Laboratoire Image Ville Environnement, UMR 7362 CNRS, University of Strasbourg, F-67000 Strasbourg, France (e-mail: clement.bressant@live-cnrs.unistra.fr).

Digital Object Identifier 10.1109/JSTARS.2024.3411304

appropriate spatial and temporal scales [30], [31]. It may capture the surface reflectance of individual trees or groups of trees across seasons. This allows for the reconstruction of growth cycles, often through the use of vegetation indices [32]. Among these indices, several studies have demonstrated that MSAVI2 is particularly suitable for urban environments with low degree of vegetation and/or nonvegetated background [33]. The temporal and spatial resolutions of satellite missions are crucial when reconstructing the phenology of urban trees [34]. A large number of well-distributed acquisitions throughout the year allow more accurate retrievals of phenological events, such as start of season (SOS) or end of season (EOS). It also directly affects duration-based phenometrics, such as the short integral of senescence season (SIOSS), whose calculation relies on at least two daily phenometrics. Hence, several studies have demonstrated the usefulness of Sentinel-2 (S2) multispectral image time series for successfully deriving such metrics in forests [35], grasslands [36], or peatlands [37]. In urban areas, the spatial resolution of S2 images (10 m) can be problematic since urban trees are identified as small elements with various morphologies (isolated ornamental trees, tree rows, small groves, etc.). Too large of a pixel captures mixed signals that provoke biased surface reflectances and homogenized interspecies signals [38]. Thus, phenological metric estimates are also biased, as they are not specific to targeted trees or groups of trees.

Recently, the PlanetScope (PS) time series has been proposed as an effective alternative to the S2 time series, especially in urban environments: the images provide high-frequency surface reflectance data (every day), suitable spatial resolution (up to 3.125 m), and interesting spectral interoperability with S2 [39], [40] for the monitoring and the mapping of individual trees [41], [42]. For example, Alonzo et al. [43] used approximately 130 PS images per year between 2018 and 2020 to investigate the drivers of earlier SOS and later EOS for  $\sim 10\,000$  species-labeled trees in the city of Washington DC. The results showed that tree species accounted for four times more variability in the timing of the SOS and EOS than did tree planting location. From a methodological point of view, the results also showed strong agreement ( $R^2 = 0.94$ ) between the SOS and the EOS derived from PS and those derived from multisource land surface phenology [44]. Nonetheless, the heterogeneity of acquisitions due to the variability in PS viewing parameters potentially represents a significant source of error in phenological parameter estimates. Indeed, since the viewing angle and sensor azimuth are not as uniform for this 430+ satellite constellation as for the two S2 satellites, the data being collected are more diffuse in terms of reflectance, requiring further consideration depending on the objectives. These aspects have been relatively unexplored until recently, while the number of studies relying on these data has been continuously increasing.

Simultaneously, the use of in situ (IS) sensors has continuously evolved, greatly promoted by sensor networks with increasingly lower acquisition, operational, and maintenance costs. These methods bridge the gap between satellite and field observations [45], [46] both in terms of spatial/temporal resolution and the granularity of the data collected. On the one hand, they can be used to validate satellite estimates or to enhance ground-based observations [47]; on the other hand, they can be used as efficient and cost-effective stand-alone observation networks [48]. In the context of urban tree phenology,

IS sensors (meteorological or soil sensors) are used to derive indirect parameters such as environmental conditions that affect plant development [49]. Other sensors allow for the retrieval of direct parameters. The most striking examples are phenocams, which are used to monitor vegetation greening or browning continuously with the systematic acquisition of RGB and/or IR images from a fixed position [50], [51], [52]. Then, images are processed to derive the time series of color-based indices (green chromatic coordinate (GCC) or red chromatic coordinate), from which phenological parameters can be estimated. R or Python packages such as *phenopix* [53] or *phenology* [54] are widely accepted tools by the scientific community for performing these tasks. They are based on a similar approach to other packages and software for analyzing satellite time series, such as famous *TIMESAT* [55] or *greenbrown* [56]. However, installing phenocams and maintaining them in urban areas can be challenging due to high human frequency and degradation. In contrast, portable sensors such as smartphones thus allow for the capture of both color and tree canopy density information [57], [58]. These methods provide high levels of flexibility in acquisitions, facilitating the retrieval of phenological parameters at large scales for a high number of sampled objects [59].

Our study aimed to provide insights into the quality of phenological estimates of urban trees derived from high-spatial-resolution satellite image time series (SITS). Our goal was first to investigate the combined effects of the type of phenometrics (daily or duration-based), phenophases, and satellite missions on the accuracy of satellite-derived estimates. Second, we aimed to improve the understanding of the RS signals above trees regarding tree development stages in the annual growth cycle derived from IS measurements. Finally, we explored the potential impacts of satellite mission characteristics on the variability of phenological estimates according to the type of phenometrics. We sought to answer the following questions.

- 1) What are the discrepancies between IS and RS-derived phenometrics for urban trees regarding different phenophases and SITS (S2 and PS)?
- 2) To what extent does the relative contribution of biophysical variables related to tree development (color and canopy closure) contribute to explaining the RS signals above urban trees across different phenophases?
- 3) How does the heterogeneity in PS acquisitions, notably related to view angle, affect the estimation of phenological metrics?

## II. MATERIALS AND METHODS

### A. Study Area and Selection of Trees

The research was carried out in the Strasbourg Urban Area in northeastern France near the border with Germany. With 33 municipalities, more than 1.3 million people live in the urban agglomeration, with a population density of 1500 people/km<sup>2</sup>. The study area covers approximately 20 km<sup>2</sup> and includes numerous land-use classes, such as densely and sparsely built-up areas, along with some natural spaces.

The urban morphology shows different urban fabrics in line with the traditional pattern of Western European urban sprawl, which is mainly structured around the Ill and the Rhine Rivers. The climate is characterized by cool dry winters and warm stormy summers [60]. Strasbourg comprises a

wide range of trees located everywhere in its territory, along main streets, in squares and parks. This is the result of several years of policies prioritizing active investments in green infrastructure projects and massive tree planting actions still in operation [61].

To monitor these trees, local services, therefore, provide an open-source database (*Patrimoine arboré 2022* ©OpenDataStrasbourg [62]) describing the 83 670 urban trees in the public area with dendrometric, species, and management information. This database was used to select our monitored “green sites” according to five criteria on which phenology can depend and criteria that can directly influence tree reflectance.

- 1) *Tree species (any cultivar)*: The reflectance phenological behavior is species related [63].
- 2) *Crown shape*: Two similar trees show different reflectance intensities depending on the width, height, and geometry of the crown influence reflectance [64].
- 3) *Tree surrounding type*: Characteristics of the soil background influence the reflectance even through canopies [65].
- 4) *Plant layout (isolated or grouped aligned)*: This reflects one specific type of management that could be responsible for variable phenology.
- 5) *Type of pruning*: Trees that are overpruned should not be selected, as this would lead to excessive changes in phenology and reflectance [66].

The green sites selected correspond to homogeneous sets of trees according to these different criteria; for the purposes of this study, these trees are deciduous trees.

Two additional spatial criteria were considered. First, each green site should be observable with a collection of S2 pixels whose spatial resolution is the coarsest used in this study. Second, green sites should be located uniformly throughout the city to cover all local climate zones (LCZs) [67], which we found to be a good indicator of urban form, allowing us to see if our sites are not located in the same environment and are, therefore, still representative of the whole urban space. Thus, they were selected along north–south and east–west axes corresponding to urban sprawl from the city center to the suburbs. Access to the sites was also considered.

Multiple correspondence analyses followed by the use of a hierarchical ascendant classification were used to select the monitored sites based on all these criteria. It was possible to extract a proportional number of sites from the generated clusters to obtain green sites that faithfully represented the diversity of trees in the city. In total, 19 green sites were selected for further analysis. The study sites are shown in Fig. 1 and described in Appendix A, with illustrations, selection criteria, and dendrometric information.

Finally, within these green sites, a sample of trees was systematically selected for IS measurements (see the next section). Some requirements were set: 1) three trees (if not an unique tree) with regular distances between them were favored (depending on the layout); and 2) each trio of trees should be at a minimum distance of 20 m from other plant species, to avoid the contamination of the RS signal of homogeneous monitored trees [68]. These methods ensure reliable (or less biased) statistical relationships between RS and IS measurements.

## B. Ground-Based Measurements

The field campaign took place over a full growing season from March 2022 to February 2023 to monitor tree growth. Our selected sites were surveyed every 10–15 days during periods of high phenological variation, such as spring (April to June) and autumn (September to November), and once per month when plant activity was lower, from approximately 7:30 A.M. to 2:30 P.M. GMT (see Fig. 2). Solar zenith hours were avoided to prevent any lens flares on the photographs, which could compromise the following data extraction process [69]. Note that the revisit periods were also estimated thanks to a phenological monitoring carried out at the same time, based on a BBCH scale for woody plants [70], [71], describing the stages of development of tree organs. It enabled us to plan the key moments for carrying out our field measurements for each site. Moreover, to make sure that the 10–15-day gap between measurements was not too wide, we estimated the average and maximum evolution of the vegetation cycle over 15-day periods (see Appendix B), using the S2 and PS satellite data as references (MSAVI2; see the next section), after interpolation and smoothing (see Section II-D). To do this, we calculated the consecutive differences in MSAVI2 values between each DOY and averaged them over a rolling 15-day window for the 80 000+ trees of the urban area, along the whole year. The result is an average change of 0.5% and a maximum of 2% of the amplitude of the phenological curves (min–max scaled for each tree). These low values ensure that the 15-day duration is appropriate for monitoring these trees in this study area. Thus, each green site was surveyed 12 times.

- 1) The leaf rate was investigated via leaf area index (LAI) measurements, which characterize the percentage of canopy openness, gap formation, and closure. The images were derived from digital hemispherical photography (DHP) with a smartphone camera (SM-A528B/DS—64 MP) equipped with a removable 180° fish-eye lens. Camera settings (see Table I) were defined according to the literature [72], [73], [74], [75], [76] and field tests, ensuring more accurate separation between tree branches/leaves and the sky using a threshold binarization technique [77]. The parameters were set to a fixed ISO sensibility, aperture, shutter speed, and white balance regime, with autofocus and 1× optical zoom. Thus, for each tree belonging to a trio of trees, four hemispherical photographs corresponding to the four cardinal points were captured with constant distance, height, and orientation of the lens as well as one hemispherical photograph in each interstice (see Fig. 1 and Appendix C). For each photograph, LAI was inferred from angular gap fraction using the complete *hemispher* R package [78]. The processing parameters were defined following a series of tests and according to the literature. We chose the Otsu thresholding method as it provided robust binarization [79], [80], based on the blue channel of the RGB hemispherical photographs for maximal contrast between vegetation elements and background (sky) [81], [82]. This thresholding step is independent for each hemispherical photographs. The maximum radius of the angular calculation rings has been reduced to limit the presence of artifacts from nearby buildings. Even with precise sensor parameters, cases of overexposure,

Green site locations and field data acquisitions schemes

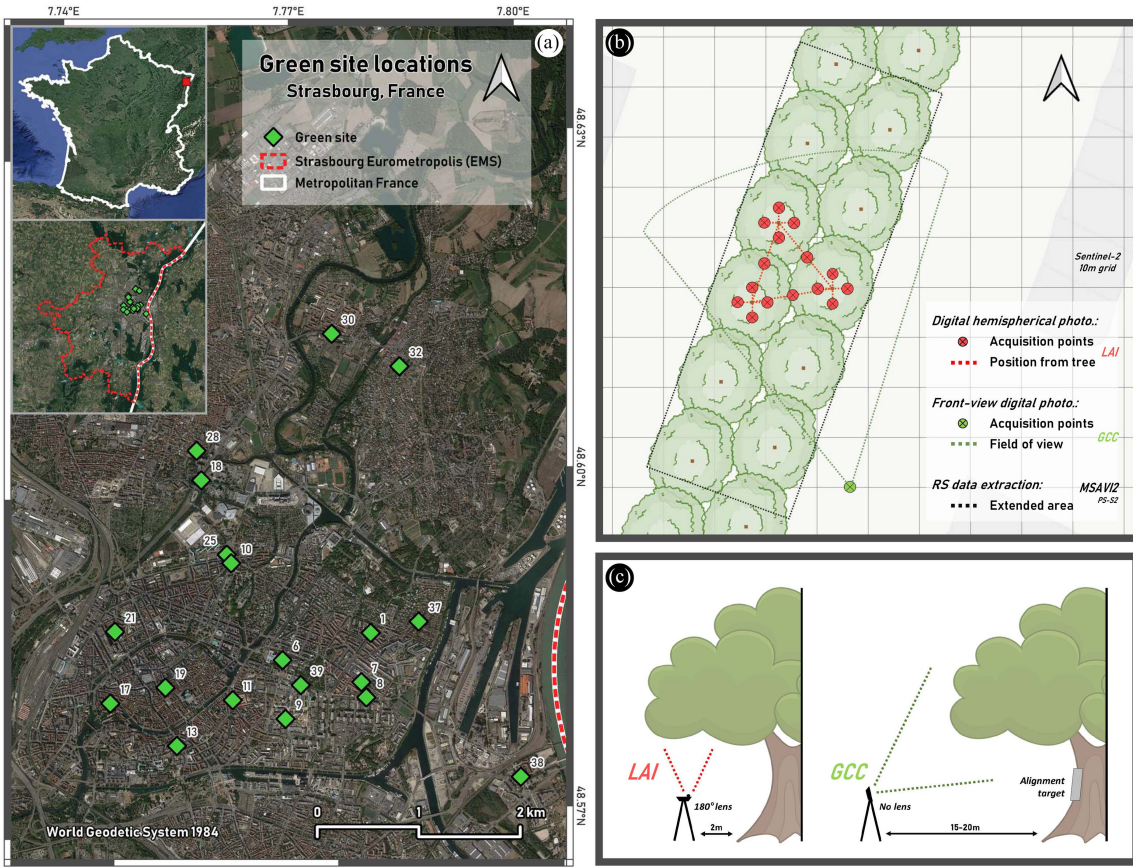


Fig. 1. (a) Green site locations in the Strasbourg Urban Area, France. (b) Site-related field data acquisition schemes for digital hemispherical photography (red), front-view digital photography (green), and extended area for RS data extraction (black). (c) Tree-related field data acquisition scheme for digital hemispherical photography (right) and front-view digital photography (left).

In situ measurements and satellite image acquisition dates

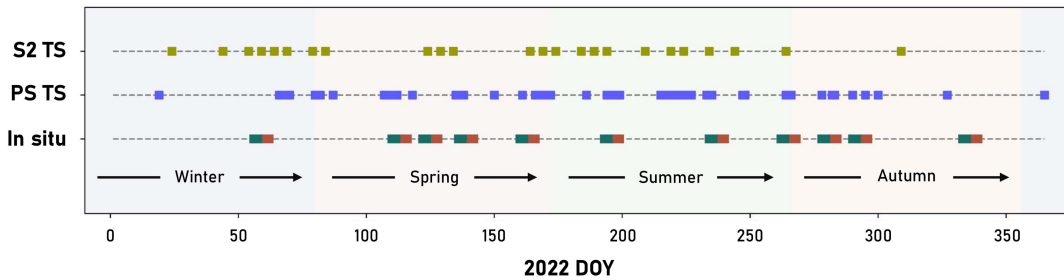


Fig. 2. IS measurements and satellite image acquisition dates (2022).

reflection, and lens flares were sometimes identified, as the incident rays are not filtered by a dense canopy as they are in forests [83]. Their presence depend on the sun orientation and the cardinal position of the sensor. Acquisition at each cardinal point for several trees and aggregation into a single value has helped to limit these biases: the median LAI was calculated from all LAI measurements and assigned to the green site (noted as LAI<sub>site</sub>).

2) Leaf color was monitored through the acquisition of GCC [84], which is a robust indicator highly correlated with photosynthetic activity [85], [86]. GCC is calculated from the digital color values as the ratio of green to the channels of an RGB sensor. Thus, one front-view photograph of 3468×4624 pixels facing north, to limit canopy shadows and glare [87], was captured for the trio of trees at each survey. The distance between the

TABLE I  
CAMERA SETTINGS FOR IS DATA ACQUISITION (SM-A528B/DS—64 MP)

	Value	Purpose	Objective
<b>ISO</b>	100	Light sensitivity	Low; to avoid the sensor being too sensitive to light, limit noise such as lens flare and poor pixel characterization at the tree/sky interface
<b>Shutter speed</b>	1/3000s	Exposure time	Fast; to avoid the sensor receiving light for too long, and to more accurately capturing leaves (canopy movement can be significant due to wind, especially in urban corridors)
<b>Aperture</b>	<i>f</i> /1.8	Size of lens opening	Wide; to allow a significant amount of light, useful when canopies are dense and low (a common case in cities). Also limited by sensor capabilities
<b>White balance</b>	5000K	Color adjustment	Neutral; to correspond to the daylight color/shade (particularly useful for next front-view digital photographs)
<b>Focus</b>	Autofocus	Sharpness	To enable clear shots to be taken at each of the sites (different tree crown heights)

shooting location and the target was optimized to enhance the field of vision of the trees (see Fig. 1 and Appendix C). Similar photographic equipment was used for the LAI measurements, and identical camera settings were used to guarantee that the monitoring was easily repeatable. We obtained the GCC values of green materials in each photograph using the interactive *phenopix* R package [53]. A value is, therefore, available on each date for each site.

### C. Satellite Image Time Series

1) *S2 Imagery and Preprocessing*: For this study, S2 images were acquired during the tree survey period. Twenty-four S2 Level-2A (L2A = atmospherically corrected surface reflectance) were downloaded from the Copernicus Open Access Hub website and corresponds to all images where at least one green site was cloud free (see Fig. 2). These S2 images, available every five days, comprise three classic visible bands and a near-infrared (NIR) band (B2, B3, B4, and B8) at a 10-m spatial resolution, and six spectral bands at 20 m from the red-edge and NIR spectral domains (B5, B6, B7, and B8a, respectively) to the shortwave infrared spectral domain (B11 and B12). Provided cloud masks and cloud shadow masks were then applied to each image. On average, each green site was observed between 23 and 24 times.

To extract the temporal signal of trees at each green site, the selected S2 image time series was first coregistered to avoid geometric misalignment between acquisitions. We used the CO-REGIS processing chain, which is particularly well suited to this sensor [88]. It relies on dense subpixel offset measurements and robust statistics to correct for systematic shifts and striping artifacts. All channels were coregistered independently. Then, spectral information was summarized using the modified soil adjusted vegetation index 2 (MSAVI2), which is dependent on the vigor and quantity of vegetation. It displays greater resilience against changing soil conditions and significantly mitigates soil interference [89], [90]. This index is better suited to highly heterogeneous urban environments than the well-known normalized difference vegetation index (NDVI) [91], [92]. It is also calculated from the red and NIR (10-m resampled NIR narrow) bands, with values ranging between  $-1$  and  $+1$ , where the higher the value, the greater the plant activity. The formula is as

follows:

$$\text{MSAVI2} = \frac{2(\text{nir} + 1) - \sqrt{(2\text{nir} + 1)^2 - 8(\text{nir} - \text{red})}}{2}$$

where “nir” is the 10-m NIR narrowband reflectance and “red” is red band reflectance. Median MSAVI2 values were calculated for each S2 acquisition at each green site from all the pixels fully included in the region of interest. This latter corresponds to the convex hull (see Fig. 1), which fits the trio of trees and is then extended to encompass neighboring trees of the green site (up to a maximum distance of 50 m, and noted after as the “tree sampling region”). The tree sampling region was manually digitized from Pléiades very high spatial resolution images (0.50 m) acquired on June 30, 2022.

2) *PS Imagery and Preprocessing*: Fifty-three PS Ortho Tile four-band products were downloaded from the Planet’s data delivery API during the same period (see Fig. 2). These Level-3A preprocessed products are atmospherically corrected surface reflectance data on demand (*analytic\_sr* assets), at a 3.125-m spatial resolution, available almost every day. The generations of PS sensors and their spectral responses were considered in this study: only the latest generation SuperDove satellite images (PSB.SD) were selected because they are natively spectrally interoperable with S2 and have, on average, almost identical and correlated surface reflectances with the blue, green, red and NIR narrowbands [39], [40] (see Appendix D).

As PS images were generated with different spatial coverages, we first merged all tiles available on each date that intersected the city boundaries. Then, to ensure geometric alignment between dates and matching statistical comparisons with the S2 time series, all available merged PS images were coregistered from the S2 grid. We used the *AROSICS* python package, which performs automatic subpixel coregistration of two satellite image datasets based on an image approach working in the frequency domain [93]. This PS and S2 coregistration, which is particularly relevant in an urban environment [94], was evaluated using time series. Linear regressions comparing the two RS sensors, for pairs of images with very close dates (less than five days), are available in Appendixes for coregistered (see Appendix E) and uncoregistered (see Appendix F) images. Fourteen pairs of dates and a total regression show that this coregistration step was beneficial. Overall, our graphs show a significant increase

## Methodology overview

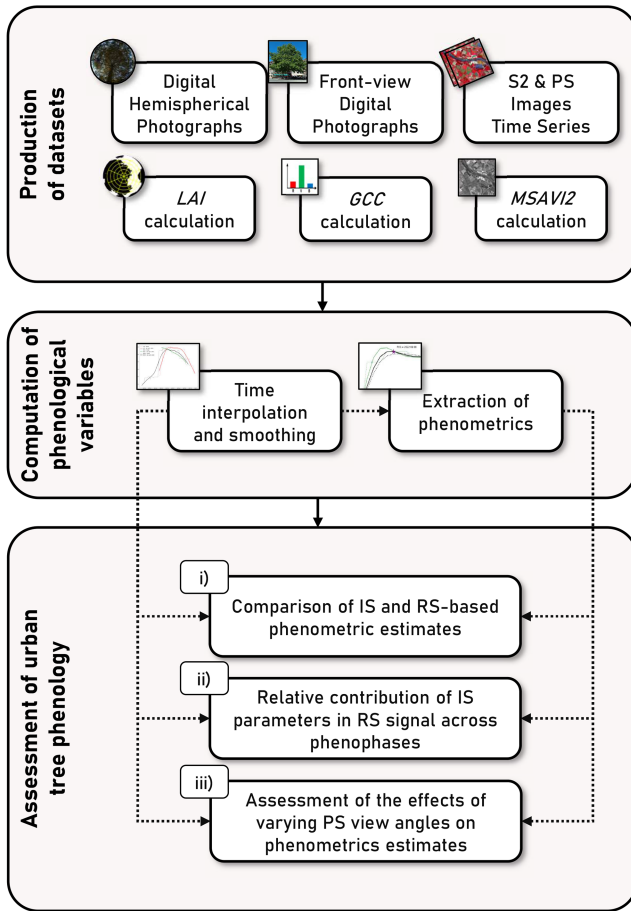


Fig. 3. Main methodological steps.

in the correlation with even an  $R^2$  rise of 4% for all 14 dates combined, as well as a decrease in the root-mean-square error (RMSE). This analysis was carried out on all the trees within the Strasbourg urban area. It should be noted that one date (S2 01/09/PS 04/09) shows a slight drop in correlation, but this does not justify the removal of images from this date. Finally, with the aim of comparing the performances of S2 and PS in reconstructing phenological parameters, MSAVI2 was also calculated for each date from the merged PS tiles. The median MSAVI2 was reported for each green site according to the same tree sampling region.

### D. IS and Satellite-Based Phenology

Once the raw data had been collected, the rest of the methodological approach is summarized in Fig. 3.

1) *Data Smoothing*: LAI, GCC, MSAVI2<sub>PS</sub> and MSAVI2<sub>S2</sub> time series were all fitted with a Savitzky–Golay filtering method to derive daily values and reduce noise introduced by undetected clouds or cloud shadings [95], [96]. The Savitzky–Golay filter is a moving window that removes outliers while preserving trends (example shown in Fig. 4). A least squares fitting convolution is used to fit and calculate derivatives of a set of consecutive values. The convolution corresponds to a weighted moving

## Data interpol. and smoothing

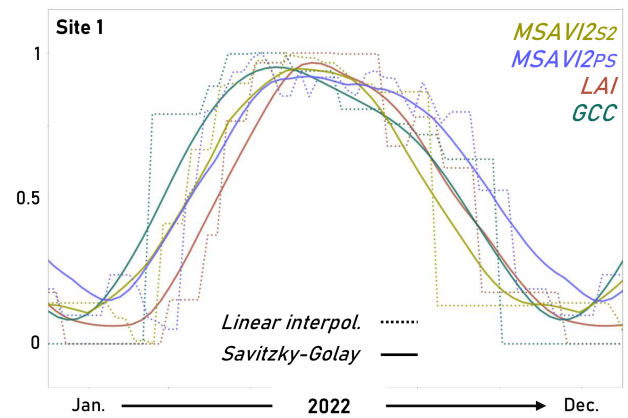


Fig. 4. Example of Savitzky–Golay interpolation and smoothing of different datasets in 2022—Site no. 1. Simple linear interpolations are also shown.

average filter whose weights vary according to a degree of a polynomial fixed by users. Regarding the weight applied, the corresponding least squares fit is performed in the moving window. In this study, a moving window of seven days was applied, as a 15-day period was considered a relatively stable period for the annual vegetation cycle. We also favored a second-degree polynomial order to seek a balance between smoothing the data and maintaining the moderate variations, which is particularly suitable for signals with relatively smooth changes [97], [98].

2) *Phenological Parameters*: Phenological metrics were calculated using a threshold-based method consisting of a pre-defined percentage of the vegetation growth/decline amplitude [55]. We used this straightforward method due to its relative simplicity and robustness and because it is the most commonly used approach by the community. We thus want to communicate our results to the largest audience.

First, for the sake of comparison, the four time series were normalized using min–max feature scaling, and the threshold values were identical for all of them. No consensus exists on threshold values for calculating phenometrics [99]; we chose amplitudes of 30% and 80%. We calculated a list of phenometrics whose purpose is diverse. One-third of these phenometrics correspond to DOY phenometric bounding phenophases, such as SOS, start of maturity (SOM), end of maturity (EOM), and EOS. The second three aim to quantify different growth durations, such as the length of growing season, length of maturity season, length of senescence season, and length of season. The last third comprises integral-derived metrics (trapezoidal rule) to measure the cumulative amount of biomass produced during the target growth period. We calculated the short integral of the growing season (SIOGS), the short integral of the maturity season (SIOMS), the short integral of the senescence season (SIOSS), and the short integral of the season (SIOS). Finally, after carrying out all the analyses on these 12 metrics (see Table II), only “daily” (SOS, SOM, EOM, and EOS) and “duration-based” phenometrics (SIOGS, SIOMS, SIOSS, and SIOS) were considered due to the similar results between length and integral-based metrics.

TABLE II  
LIST OF THE DAILY AND DURATION-BASED PHENOMETRICS CALCULATED AND USED IN THIS STUDY

	Code	Name	Method
Daily phenometrics	SOS	Start Of Season	Day of the year at 30% growth slope threshold
	SOM	Start Of Maturity	Day of the year at 80% growth slope threshold
	EOM	End Of Maturity	Day of the year at 80% decline slope threshold
	EOS	End Of Season	Day of the year at 30% decline slope threshold
Duration-based phenometrics	SIOGS	Short Integral Of Growing Season	Area under the curve between SOS and SOM
	SIOMS	Short Integral Of Maturity Season	Area under the curve between SOM and EOM
	SIOSS	Short Integral Of Senescence Season	Area under the curve between EOM and EOS
	SIOS	Short Integral Of (full) Season	Area under the curve between SOS and EOS

### E. Statistical Analysis

1) *Measuring Discrepancies Between IS and Satellite-Based Phenometrics*: A regression-based analysis was performed to measure discrepancies between IS (LAI and GCC) and satellite-based phenometrics (S2 and PS) according to different phenophases.  $R^2$  and statistical significance were used to measure how well the IS variable could explain the variation in the RS variable. The RMSE was also calculated to investigate how well the resulting regression model could predict the value of the RS variable.

2) *Evaluating the Contributions of Biological Parameters to RS Phenological Signals*: To address the contribution of biological parameters to the RS signals above trees during the growing season, a hierarchical partitioning procedure was applied using the R packages *lme4* and *partR2*. This allows us to assess the independent and joint contributions of each explanatory variable in a linear model. Thus, we calculated a linear mixed model with MSAVI2 as a response variable and IS LAI and GCC as fixed variables for three phenophases, namely, the growing [SOS-SOM], maturity [SOM-EOM], and senescence [EOM-EOS] seasons, for the S2 and the PS time series. The ID sites were set as random variables to control for pseudoreplication.

For each model, we applied the following procedure.

- 1) A number of days was randomly sampled in each phenophase for each site. As the length of phenophases was different for each green site, this number is equal to the minimum number of days observed among sites.
- 2) The latter random sampling was performed following a stratified sampling strategy based on quantiles to ensure that the input datasets covered the entire phenophase.
- 3) One hundred runs of 50 parametric bootstrap iterations were performed, and the mean partial (semipartial)  $R^2$  and  $p$  value were used to measure the relative contribution of each IS variable.

3) *Assessing the Effects of Variable View Angles of PS Scenes on the Resulting Phenometrics*: We used Monte Carlo (MC) simulations to investigate the effects of the variability of view angles in PS acquisitions on the accuracy of the derived phenometrics. MC simulations are generally used when processes are random or when assumptions in theoretical mathematics are not well known [100], [101]. In this study, applying MC simulations showed several advantages. First, we are not aware of the amount of error induced by variable view angles of PS scenes on tree surface reflectances over the year. Second, MC simulations are easily performed and applicable to different ecological habitats. This approach could thus make more systematic the analysis of

satellite data quality on derived environmental variables such as phenometrics.

The first step consisted of calibrating the range of error where the error was randomly sampled and assigned to MSAVI2 values at each date. To perform this stage, we used an approach based on the darkest pixel principle applied in the context of atmospheric corrections [102], [103]. It consists of calculating an error value by examining the variability of pixels that are not expected to change over time. Therefore, 1000 spatial points from MSAVI2<sub>S2</sub> (1/500 of the total number of pixels) were selected in Strasbourg in areas with stable annual surface reflectance. These areas correspond mainly to stagnant inland water bodies. We then calculated the standard deviation of all MSAVI2<sub>PS</sub> values recorded throughout the year at each point (annual point error) and calculated the mean of these latter values (mean error). Finally, the normal distribution of the error was calculated by averaging the mean error and calculating the standard deviation of the annual point error. Hence, for each run (1000 runs in total), a specific value of error was randomly extracted from the normal distribution to add it to the median MSAVI2<sub>PS</sub> values at each green site on each date. New MSAVI2<sub>PS</sub> time series were thus drawn at each run, and new phenometrics were derived.

Boxplot distributions were ultimately investigated to analyze the variability after 1000 runs, with standard deviations, to measure the latter effects on output daily phenometrics. The relative uncertainty percentage [104] was calculated to investigate the variability of estimates in duration-based phenometrics. Specifically, we used the 95% uncertainty percentage that involves the 95% confidence interval, as follows:

$$95\% \text{ uncertainty} = \frac{1}{2} \left( \frac{95\% \text{ confidence interval width}}{\text{mean}} \right) \times 100.$$

Then, a threshold of 25% was set, above which the uncertainty was considered too high for considering reliable estimated duration-based phenometrics.

## III. RESULTS

The results are again divided into three sections, aimed at answering our three main questions: 1) the discrepancies between RS and IS-derived phenometrics; 2) the relative contributions of IS GCC and LAI to the RS signals above trees across phenophases; and 3) the effects of the heterogeneity in PS acquisitions on phenological estimates.

### A. Discrepancies Between RS and IS-Derived Phenometrics

The regression results between the phenometric estimates derived from satellite time series and those derived from IS data

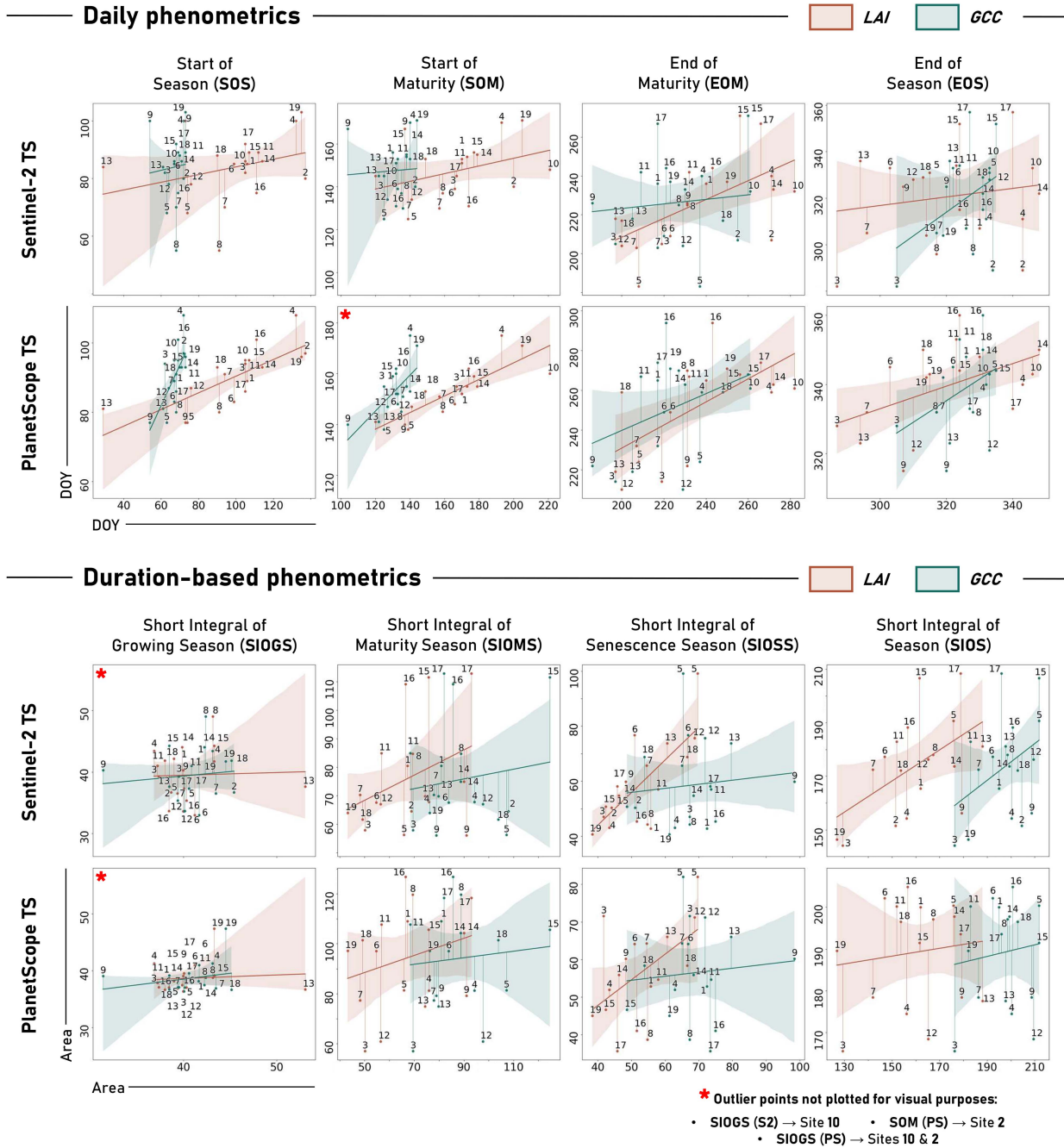


Fig. 5. Linear regression model comparisons of daily and duration-based phenometrics for observed (LAI—red and GCC—green) and predicted values (S2 and PS).

are presented in Fig. 5 and Table III. First, our findings indicated that daily phenometric estimates derived from the  $MSAVI2_{PS}$  time series exhibited greater correlations with IS estimates than did the metrics derived from  $MSAVI2_{S2}$ . The average  $R^2$  values were  $0.51 \pm 0.18$ , and all the statistical relationships associated with the different phenometrics (e.g., SOS, SOM, and EOM) were significant except for those associated with the EOS. In contrast, the  $R^2$  values for the four phenometrics calculated with S2 averaged  $0.19 \pm 0.19$ . Only the EOM estimates derived from the latter satellite missions exhibited a significant relationship

with the IS LAI-derived estimates. We found very little significant agreement between the satellite-based and IS duration-based phenometrics, indicating strong error propagation for metrics relying on several daily phenometrics (first and last days). Only the SIOSS estimates derived from IS LAI showed significant relationships with those calculated with both the  $MSAVI2_{S2}$  and  $MSAVI2_{PS}$  time series ( $R^2 = 0.66, p = 0.0020$  and  $R^2 = 0.43, p = 0.0188$ ). A significant relationship was also found between the SIOS estimates derived from  $MSAVI2_{S2}$  and the IS LAI.



TABLE III  
REGRESSION RELATIONSHIPS BETWEEN SATELLITE DATA (S2 AND PS) AND IS DATA (LAI AND GCC) FOR ALL DAILY AND DURATION-BASED PHENOMETRICS

		Sentinel-2 TS			PlanetScope TS		
		$R^2$	$p$	RMSE	$R^2$	$p$	RMSE
SOS	LAI	0.13	0.2300	27	0.75	0.0003***	21
	GCC	0.01	0.7913	17	0.69	0.0013**	23
SOM	LAI	0.32	0.0943	21	0.48	0.0115*	14
	GCC	0.00	0.8422	18	0.37	0.0316*	27
EOM	LAI	0.54	0.0066**	17	0.69	0.0014**	20
	GCC	0.02	0.6607	18	0.34	0.0390*	29
EOS	LAI	0.27	0.0897	15	0.44	0.0161*	23
	GCC	0.23	0.0975	6	0.30	0.0554	14
SIOGS	LAI	0.00	0.9927	10	0.01	0.7355	11
	GCC	0.02	0.6652	3	0.20	0.1202	3
SIOMS	LAI	0.34	0.0852	10	0.06	0.3981	28
	GCC	0.03	0.5448	20	0.00	0.9170	17
SIOSS	LAI	0.66	0.0020**	7	0.43	0.0188*	4
	GCC	0.01	0.7950	13	0.09	0.3199	15
SIOS	LAI	0.44	0.0166*	16	0.02	0.6588	33
	GCC	0.24	0.0880	24	0.02	0.6157	13

Statistical significance is shown as follows : \* $p < 0.05$ ; \*\* $p < 0.01$ ; \*\*\* $p < 0.001$ .

TABLE IV  
SEMPARTIAL  $R^2$  VALUES OF LAI, GCC, AND SHARED AMONG THEM (%) ON DEPENDENT SATELLITE VARIABLES (S2 AND PS), ALONG THREE PHENOPHASES

		Sentinel-2 TS			PlanetScope TS		
		part $R^2$	Lower CI	Upper CI	part $R^2$	Lower CI	Upper CI
Growing Season	LAI+GCC	98.6	98.5	98.6	97.0	96.9	97.1
	LAI	45.1	41.1	46.6	9.2	7.1	10.3
	GCC	14.9	9.0	17.3	0	0	0
Maturity Season	LAI+GCC	41.1	39.3	42.3	53.0	51.3	54.4
	LAI	30.9	28.7	32.9	35.5	33.4	36.9
	GCC	27.5	25.3	28.9	22.0	18.8	23.8
Senescence Season	LAI+GCC	95.3	95.1	95.5	98.7	98.6	98.7
	LAI	23.3	19.9	24.8	16.1	11.5	17.9
	GCC	35.9	32.2	37.4	30.8	26.6	29

Second, the phenological estimates calculated with IS LAI values exhibited greater correlations with satellite-derived estimates than did the estimates obtained with IS GCC. The mean  $R^2$  values obtained via regression between the daily phenometrics derived from MSAVI2<sub>PS</sub> and the IS LAI are equal to  $0.59 \pm 0.15$  against  $0.43 \pm 0.18$  with the IS GCC. Similarly, the agreement between the daily phenometrics obtained with S2 and the IS LAI displayed an average  $R^2$  of  $0.32 \pm 0.17$  against  $0.06 \pm 0.11$  for the GCC. However, these results should be nuanced because the RMSE values were not always lower for the LAI-derived estimates than for the GCC-derived estimates. For example, the RMSEs resulting from the residuals of the linear regressions between daily phenometrics estimated with GCC and MSAVI2<sub>S2</sub> were smaller than those obtained when estimates were derived from LAI time series in three out of four cases (e.g., SOS, SOM, and EOS). Third, discrepancies between satellite- and IS-derived phenological estimates vary across phenophases. When selecting significant regression models between IS and satellite estimates, we observed greater correlations during the initial stage of growth and at the end of the maturity period. Linear models between the SOS and the EOM estimated from MSAVI2<sub>PS</sub> and IS LAI showed  $R^2$  values of approximately 0.70 (0.75 and 0.69, respectively). These values were lower than 0.50 for models aimed at estimating the SOM and the EOS (0.48 and 0.44, respectively).

### B. Relative Contributions of IS GCC and LAI to the RS Signals Above Trees Across Phenophases

As expected, in Fig. 6 and Table IV, the results of hierarchical partitioning showed joint contributions close to 90% for two-thirds of models, indicating strong collinearity between GCC and LAI. Nonetheless, the resulting average limits of confidence intervals featuring independent contributions do not intersect with 0, except for GCC in the growth period with the PS time series. This allows for the analysis of the relative influence of IS biophysical parameters on the variance of satellite-based MSAVI2 signals. We found that the LAI exhibited a stronger independent contribution than the GCC in the first two periods, while the opposite effect was observed for the senescence phase. These findings were consistent between satellite missions, and some key points should be highlighted. First, the contributions of both parameters were almost equal for the maturity season when explaining the variation in MSAVI2<sub>S2</sub>. In contrast, more than a ten-point difference in favor of LAI was observed when considering MSAVI2<sub>PS</sub>. The joint contributions are the lowest of the three phenophases with 41.1% and 53.0% for S2 and PS, respectively, indicating that the set of predictors as a whole is not explaining much of the variation in the dependent variable during maturity season. Next, we found null and very low contributions of the GCC and LAI parameters, respectively (contribution scores = *Oslash*; and 0.09), to the variance in MSAVI2<sub>PS</sub> during

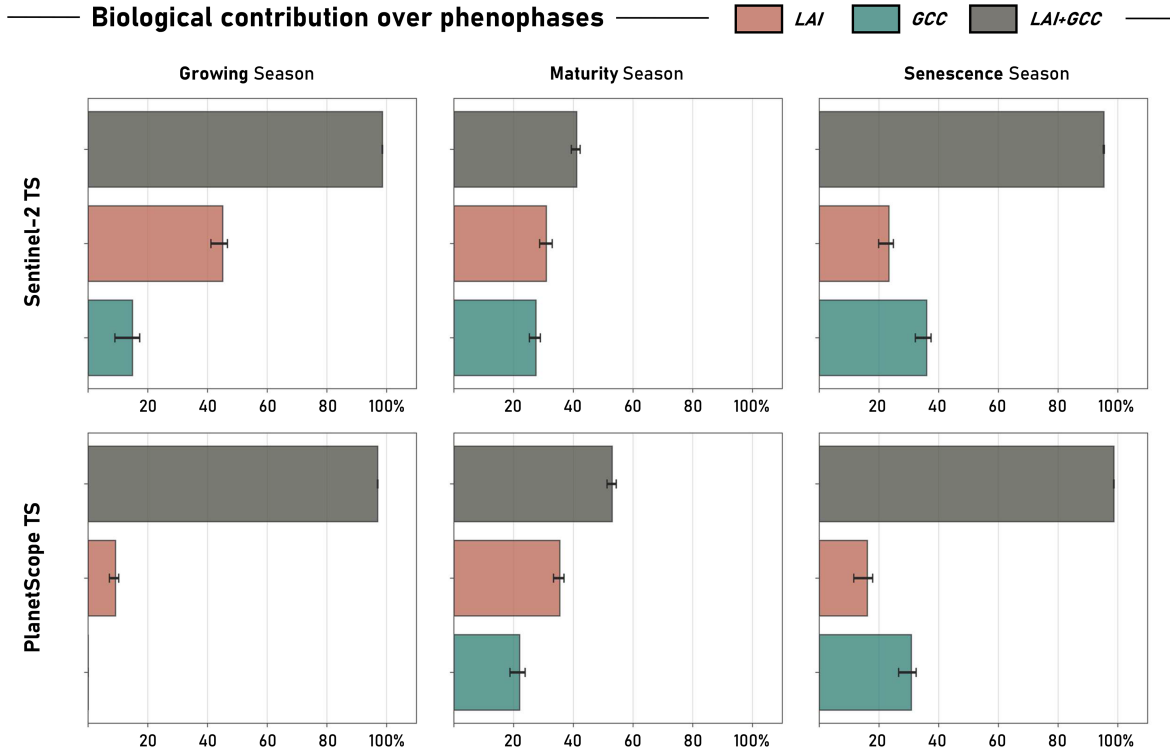


Fig. 6. Bar chart of semipartial  $R^2$  values for each specific predictor (LAI—red and GCC—green) and shared among them (gray) for the two time series (S2 and PS) along three productive phenophases.

TABLE V  
AVERAGE VALUE OF PS-DERIVED SIMULATED DAILY PHENOMETRICS FOR EACH SITE, WITH STANDARD DEVIATION

	SOS	SOM	EOM	EOS		SOS	SOM	EOM	EOS
<b>1</b>	88±2	152±2	263±7	348±4	<b>11</b>	93±2	156±3	265±8	353±4
<b>2</b>	95±3	260±5	315±2	370±2	<b>12</b>	87±2	147±2	210±4	322±5
<b>3</b>	94±2	156±2	214±4	329±7	<b>13</b>	81±2	141±2	220±8	324±5
<b>4</b>	108±3	176±2	257±6	341±4	<b>14</b>	93±3	156±3	260±8	350±5
<b>5</b>	76±2	138±2	222±16	343±5	<b>15</b>	95±3	160±4	265±5	344±5
<b>6</b>	83±2	148±2	248±8	345±3	<b>16</b>	101±5	174±9	280±8	365±6
<b>7</b>	90±2	152±3	230±9	334±5	<b>17</b>	85±4	158±6	272±4	335±5
<b>8</b>	79±4	147±4	261±10	337±4	<b>18</b>	93±2	154±3	253±13	351±5
<b>9</b>	76±2	140±2	222±7	319±4	<b>19</b>	95±2	172±3	270±4	343±3
<b>10</b>	94±2	160±2	260±5	345±4	<b>Mean st.dev.</b>	2.6±0.9	3.1±1.7	7.2±3.4	4.5±1.0

The mean standard deviation is also included.


the growth period. However, their joint contribution was close to 100%, demonstrating that it was not possible to disentangle the effects of GCC and LAI in the MSAVI2<sub>PS</sub> variance for this configuration. In contrast, the LAI showed a contribution three times greater than that of the GCC (45% against 15%) according to the S2 time series for the same period. Finally, GCC had a greater relative influence than LAI on the MSAVI2 variance for both missions during the senescence season, reaching more than 30%. This was true despite contribution scores lower than those observed with the PS time series. The joint contributions are almost as important as for the growing phenophase.

C. Effects of the Heterogeneity in PS Acquisitions on Phenological Estimates

Our simulation results allow for the assessment of the effects of variable view angles in PS scenes on phenological estimates.

These results were considered in two steps: one focusing on standard deviations derived from 1000 simulations for daily phenometrics (see Fig. 7 and Table V) and the other on relative uncertainty results for duration-based phenometrics (see Fig. 8).

Overall, we found that the standard deviation results for daily phenometrics ranged from low to high, with averages ranging from 2.6±0.9 for the SOS metric to 7.2±3.4 for the EOM metric. Specifically, we noted greater variability in the estimates of late-season metrics than in those of early-season metrics (see Table V). The combined SOS and SOM data had an average resulting standard deviation equal to 2.9±1.4 among the sites, compared to 5.8±2.9 for the EOM–EOS pair. For these specific late-season metrics, nearly half of the sites exhibited standard deviations exceeding 1 week for the EOM metric, with a maximum occurring at 16 days for site number 5. However, the EOS metric exhibited more moderate variability, with no recorded standard deviation exceeding seven days and an average of

PS TS daily phenometrics simulation 5%  95%

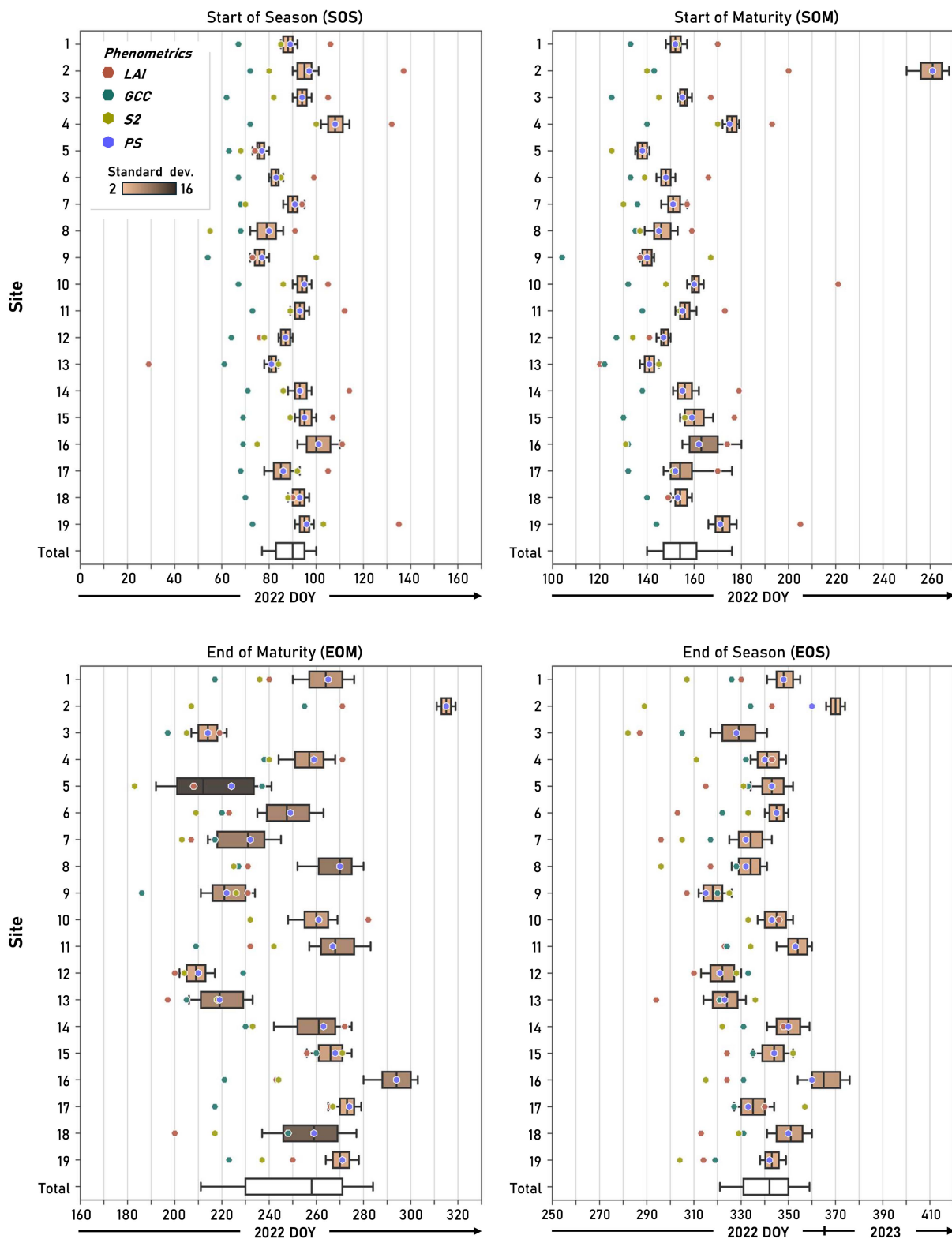


Fig. 7. Distribution of MC simulated daily phenometrics on the PS TS with 5–95% percentiles. The original phenometrics of our study are also shown (LAI, GCC, S2, and PS), and boxplots are colored depending on the standard deviation.

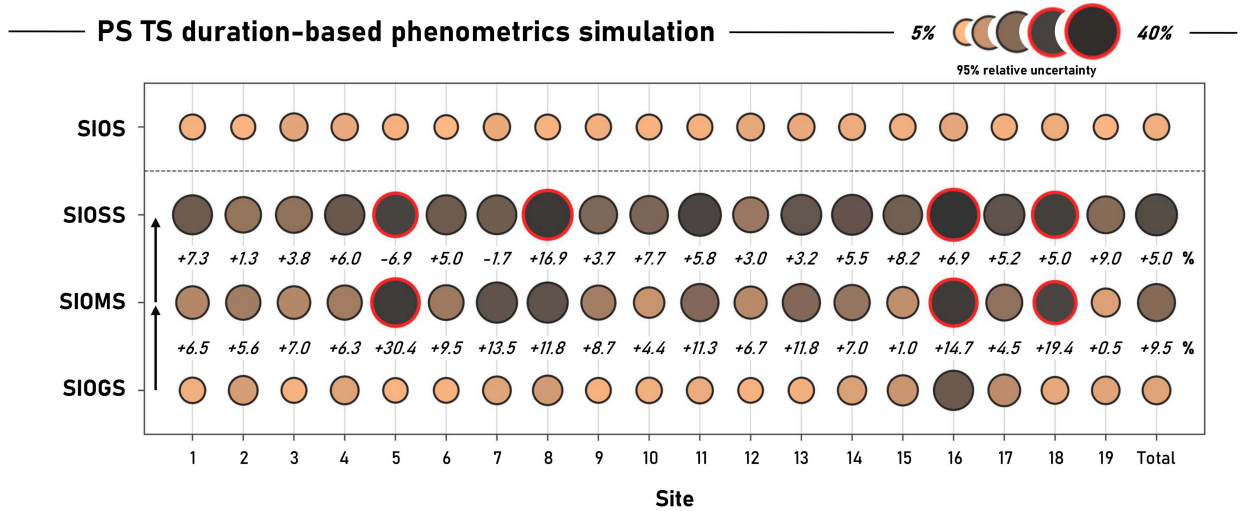


Fig. 8. Proportional representation of the dispersion of PS TS-simulated duration-based values around the mean, with 95% relative uncertainty percentage. The three seasons (SIOGS, SIOMS, and SIOSS) are represented as well as for the total season (SIOS). Percentage changes over time between two seasons are given, as well as the  $>25\%$  uncertainty values (red circles), which we define as a cutoff threshold for considering reliable estimated duration-based phenometrics.

4.5 $\pm$ 1.0 days. Finally, the boxplot distributions in Fig. 7 also allowed us to consider gaps with S2 and IS-derived estimates. We found average absolute differences equal to  $|6|\pm 12$  and  $|13|\pm 29$  days between the median values resulting from 1000 simulations and the S2-derived estimates of the SOS and SOM values, respectively. These differences ranged from  $|26|\pm 25$  to  $|21|\pm 26$  for the EOM and the EOS. Concerning gaps with IS variables, differences between median values calculated from simulated distributions, and LAI- and GCC-derived estimates, were relatively more constant among the four phenometrics. These values were, respectively, equal to  $|10|\pm 20$ ,  $|8|\pm 24$ ,  $|15|\pm 21$ , and  $|22|\pm 16$  with LAI, and  $|23|\pm 6$ ,  $|28|\pm 23$ ,  $|26|\pm 24$ , and  $|15|\pm 12$  with GCC.

Fig. 8 shows proportional circles illustrating the percentage of relative uncertainty in the simulated duration-related variables. Overall, 25% of the sites (four out of 19) exhibited relative uncertainty scores exceeding the 25% threshold (highlighted in red). These high scores were exclusively associated with either the SIOMS or SIOS metric, underscoring the significant impact of the variability in the viewing angle of PS on the quality of phenological estimates for duration-related phenometrics. Furthermore, we noted a progressive increase in relative uncertainty percentages as the growth cycle advanced. On average, there was an increase of  $9.5\pm 6.9\%$  between SIOGS and SIOMS and  $5.0\pm 4.7\%$  between SIOMS and SIOSS across all sites. Notably, the maximum relative uncertainty recorded was for SIOSS (41.9%), with an overall metric average of  $22.6\pm 7.4\%$  for this metric across all sites. Finally, SIOGS and SIOS displayed consistently low relative uncertainty percentages, averaging  $8.1\pm 3.5\%$  and  $6.3\pm 0.8\%$ , respectively. For these latter phenometrics, the impact of varying angles in PS scenes on the accuracy of estimates appears negligible.

#### IV. DISCUSSION

In this study, we aimed to investigate the quality of phenological metrics of urban trees derived from high-spatial-resolution

SITS. For this purpose, we used IS phenological metrics derived from portable low-cost images. The SITS proved to be a relevant variable for deriving accurate phenometrics of urban trees for different species in different urban contexts. Specifically, the PS time series provided the highest accuracy in phenological estimates, with variable performances across phenophases. Overall, the type of phenometrics and phenophases are the main drivers of discrepancies between RS and IS data.

##### A. SITS, Such as S2 and PS, Are New Reliable Tools to Retrieve Phenological Metrics of Urban Trees

The relationships between the RS-derived metrics and IS-derived metrics (GCC and LAI) exhibited high agreement between the S2 and PS data for the different phenometrics. Our results demonstrated the potential of the SITS for monitoring phenology in urban trees of different spatial arrangement at the city scale. These findings provide insights into satellite-based studies dedicated to environmental monitoring in complex heterogeneous environments.

The outcomes showcased the ability of SITS with a resolution of a few meters to track tree clusters and large unique trees in highly heterogeneous environments, such as urban areas. The S2 and PS time series provided consistent signals for both tree alignments and clusters within any type of tree layout within squares, parks, or streets, belonging to the same species. Consequently, reliable interspecies signals can be obtained, allowing us to observe the heterogeneity of phenology within the urban matrix. These findings are in line with recent results from Granero-Belinchon et al. [105], who successfully used the S2 series to reconstruct the phenological dynamics of urban trees exposed to different environmental conditions in Toulouse, France. These findings also support those of Alonzo et al. [43], who leveraged the PS series to investigate the SOS and EOS of numerous trees in Washington, DC. In the latter study, the results underscored the possibility of using these data to retrieve phenological indicators in heterogeneous environments

previously avoided due to low vegetation cover [106], [107]. Combined with our results, these works also ensure the ability of PS to investigate unique plant functional types and to avoid biases related to subpixel mixing in the phenometric retrieval process. Finally, our study highlights the ability of PS time series to upscale observed phenological data from the field [29], [108], [109]. These relationships were consistent with the IS GCC and LAI data across seasons, which reinforces the interest in coupling these data to investigate phenology at different spatial scales [110]. This could be a key parameter in the implementation of management-based decisions [111].

The temporal resolution of a few days demonstrates satisfactory performance in the derivation of phenometrics for objects with rapidly changing behavior within key periods. First, this indicates that the general preprocessing framework (smoothing, coregistration) effectively addresses data inconsistencies over time and yields reliable temporal signals [112]. In this regard, we recommend its systematic application in studies aiming to use these time series for urban tree phenology monitoring. Furthermore, although a sufficient number of S2 acquisitions have been processed [34], the higher temporal resolution of PS was particularly crucial, specifically for the retrieval of duration-based phenometrics. These specific metrics performed significantly better than did those obtained with S2, limiting the propagation of errors when multiple metrics were combined. Nonetheless, despite the strict selection of scenes, our simulation results showed that the variability in PS viewing angles could be a significant error source in phenological estimates [113]. The models demonstrated varying effects depending on the metric, season, and selection criteria such as species (through site). Further studies should investigate the tradeoff between the number of PS scenes available within seasons and the variability in viewing parameters for the retrieval of phenometrics. Overall, we also encourage the scientific community to delve into the impact of PS acquisition heterogeneity on the retrieval of environmental variables. Despite these challenges, our study demonstrated in a quantitative way that PS data are effective at reconstructing daily phenometrics with acceptable errors across seasons. This paves the way for a more systematic use of these data for urban phenology [114].

### *B. Phenophases and Type of Phenometrics Are Essential Drivers to Explain the Variable Quality of Phenological Estimates*

First, our results showed that duration-based phenometrics consistently exhibited greater discrepancies than did daily metrics with IS-derived metrics, regardless of the targeted mission. This reflects that the error propagation resulting from the daily metrics estimates affects metrics combining multiple ones. We found this true for metrics aiming to characterize specific periods, such as maturity or senescence. We hypothesize that their short amplitude exposed them to greater uncertainty. Conversely, simulation outcomes showed less pronounced results for metrics characterizing the entire growth cycle with a lower relative uncertainty. This means that metrics displaying lower sensitivity due to larger amplitudes are less subject to error propagation. Despite these results, the difference in the number of days

compared to IS phenometrics can still be high and still remains problematic for further analysis.

Second, simulation results demonstrating the effect of variable viewing angles in the PS time series showed increasing errors with advancing phenological cycle. This led to lower performances for EOS metrics than those obtained in spring. Our findings corroborate several studies that have already demonstrated the highest errors in the phenological retrieval process during autumn [45], [115], [116], [117]. We hypothesize that such observations are due to several reasons.

- 1) The shape of the curve at the corresponding time where phenometrics are investigated exhibits an amplitude or slope that makes threshold-based retrieval a challenging task [118]. While the growth period displayed a rapid increase in the vegetation indices during a short period followed by a well-stable maturity plateau, we observed a more progressive and/or slower period of decline for immune senescence. Consequently, the systematic threshold value applied to retrieve daily phenometrics will be more uncertain because of the elasticity of the period due to shorter or longer periods provoked by earlier or later senescence.
- 2) The duration and frequency of the RS time series in autumn are too low to monitor complex and abrupt changes. In autumn, leaves progress through different colors (green to yellow to red), thus explaining greater discrepancies between RS and IS variables [29].

Third, we explored the latter aspect in depth by studying the relative contributions of biological parameters (color and canopy closure) to the variance in the satellite-based MSAVI2. Our results showed the opposite trend in terms of the contributions of these two parameters over time, indicating that the RS signal was first related to canopy closure at the start of the season, while leaf color guided its evolution during senescence. Our results are in line with those obtained by Huemmrich et al. [119]. The latter authors noted considerable differences in the effects of ecological change on the NDVI responses in high-latitude ecosystems due to varying canopy structures. They concluded that NDVI changes associated with ecological change are most often observable at low green plant coverage or low LAI values, which is consistent with our observations. Taken together, these findings reinforce the interest in using high-resolution images since small pixels are more useful for monitoring leaf surface changes and providing more accurate phenometrics, especially in heterogeneous environments [120]. The city is one such environment, and being able to derive precise information about the colorimetry of foliage is a major asset. For example, managers can use predictive results to plan maintenance work such as pruning and general monitoring of trees. Similarly, changes in the chemical composition of leaves obviously lead to systematic variations in the ecosystem services provided. As a result, trees in the city can be detected with a view to estimating their maximum contribution periods to the environment, which is often linked to the species [43], [121]. New tree planting by decision makers will be based, for example, on estimates of the length of the seasons using satellite data, in order to optimize the benefits of trees over the maximum period of time so sought after in this changing climatic context. The results also encourage thinking about the optimization of the number of satellite scenes in

autumn for capturing rapid color changes. Synergistic effects between S2 and PS appear to be a potential solution to these challenges [122], [123], [124]. Finally, even if the quality of phenological estimates remains high in spring, challenges exist in the real monitoring of leaf color changes during the latter period. The ability of RS missions to capture these microvariations is likely to provide insights into the phenology of urban trees. Tradeoffs between citizen sciences and satellite estimates could also be relevant for performing this task [125], [126].

### *C. Coupling Satellite-Based and Portable Low-Cost Acquisitions of Phenological Estimates Help Measuring the Quality of the Essential Environmental Variables*

The accuracy of RS products has been markedly enhanced by the continuous advancements in aerospace technology for several decades now. As we have shown, despite these improvements, inherent errors in phenological estimates persist. Assessment of urban trees is challenging due to limitations stemming from the technical capabilities of satellite platforms and sensors (e.g., spatial, spectral, and temporal resolutions, view angle variations, etc.). A validation process is then essential for building confidence in the utility of RS data and ensuring its reliability [127], [128]. Systematically scrutinizing and confirming errors through reference data, such as IS measurements, assumes a pivotal role. Ground-level measurements serve as a crucial benchmark for validating the performance of high-resolution time series [129], [130]. This way, by assessing the agreement with both sources of observations, discrepancies or inaccuracies in phenological estimates can be identified and addressed [131]. Scale differences between satellites and IS measurements will always remain a complex scientific challenge [29], [132]. Nonetheless, this still can be seen as an asset to improve the overall quality of environmental data and, more importantly, to contribute to the widespread application of RS products. We were, for example, able to demonstrate differences linked to phenophases and the type of sensor using this process, which will help the scientific community get closer to the ground truth using such data in further applications.

Portable low-cost devices, such as ground sensors or smartphones, enable on-the-ground measurements with high temporal and spatial precision. It is particularly valuable in resource-constrained settings [133] and could be in complex environments such as cities, where field monitoring infrastructure may be limited. By leveraging cost-effective technologies, this approach democratizes access to critical environmental monitoring tools, fostering a more inclusive and globally informed understanding of the trees' health and development. Their flexibility, ease of deployment, and community engagement potential make them more and more valuable for real-time monitoring of environmental conditions. It could provide researchers, policymakers, and local communities more reliable information for decision making. In this study, we deliberately chose to use this type of sensor. The field acquisition protocol we defined proved feasible for collecting reliable and usable data. There is currently no study on urban trees that has gathered data over a complete phenological cycle, for two distinct biological parameters: leaf vigor linked to photosynthetic activity (GCC) and leaf area coverage (LAI). Until now, these indicators were compared with

satellite data at specific points in time [134], [135] or in an open environment [136], [137]. For the reasons mentioned earlier, we took advantage of this innovative temporal approach, which played a key role in understanding seasonal changes in this urban component.

## V. CONCLUSION

This study marks a significant stride in advancing our comprehension of urban tree phenology by amalgamating SITS from S2 and PS, alongside on-the-ground observations using portable low-cost sensors. The results underscore the potential of SITS in capturing the intricate phenological dynamics of urban trees, providing insights crucial for urban environmental management and policy formulation. Our analyses demonstrate that both S2 and PS datasets can reliably yield phenological metrics across diverse urban tree species and settings. Notably, the PS time series exhibited superior accuracy in estimating phenological events, potentially attributed to its higher temporal and spatial resolution. This characteristic proved indispensable in precisely documenting rapid phenological changes, particularly during critical transitional periods such as spring. The study also sheds light on challenges and limitations inherent in RS of urban tree phenology. Notably, we evaluated the impact of viewing angle variability in PS data as a factor influencing the accuracy of phenological estimates. While error propagation in duration-based phenometrics was highlighted, errors due to variations in satellite angles were deemed more acceptable for daily metrics. These findings provide a road map for future methodological enhancements in urban tree monitoring through RS. Furthermore, the study delves into the contribution of biological parameters (LAI and GCC) and the comparison of IS and RS metrics, revealing disparities between phenophases. The early season, characterized by more abrupt changes and a simpler phenological reconstruction, exhibited superior performance. The integration of IS measurements through portable low-cost devices emerges as a valuable approach for validating satellite-derived phenological metrics. This synergy between satellite and ground-based observations not only improves the accuracy of phenological estimates but also democratizes the environmental monitoring process, making it accessible and feasible in diverse urban settings. In summary, this research significantly contributes to the field of urban tree phenology by showcasing the effectiveness of combining RS and ground-based approaches. It introduces new possibilities for urban environmental monitoring and management, presenting a model that can be replicated and adapted in various urban contexts globally. The insights from this study underscore the importance of continuous innovation and the integration of multiple data sources in environmental research. Looking forward, future research should concentrate on refining methodologies to address specific challenges identified in this study, such as error propagation in duration-based metrics. In addition, broadening the scope of the study to encompass a wider array of tree species and urban settings would provide a more comprehensive understanding of urban tree phenology. Leveraging advancements in RS technology and data processing algorithms will be crucial for enhancing the accuracy and applicability of phenological monitoring in urban environments.

APPENDIX A

TABLE VI  
GREEN SITE DESCRIPTION WITH SPECIES, MANAGEMENT, AND DENDROMETRIC INFORMATION (IN METERS); ILLUSTRATIONS FROM JULY AND AUGUST 2022

ID	Species			Image
	Layout	Form	Base	
DBH (m)	Crown width (m)	Height (m)	Maintenance LCZ	
1	Platanus x acerifolia			
Double central alignm.	Reconversion	Stabilized	Routine	
0.50 – 0.63	10.39 – 11.18	15.00 – 16.00	Bare rock-paved	
2	Tilia tomentosa			
Quad. central alignm.	Pruned	Grassed	Routine	
0.34 – 0.36	5.26 – 6.45	6.00 – 7.00	Sparsely built	
3	Aesculus hippocastanum			
Simple two-sided alignm.	Pruned	Stabilized	Routine	
0.28 – 0.33	5.82 – 6.81	9.00 – 10.00	Compact lowrise	
4	Tilia x euchlora			
Grove	Pruned	Stabilized	Routine	
0.23 – 0.44	4.68 – 5.76	10.00 – 11.00	Compact midrise	
5	Tilia tomentosa			
Double central alignm.	Free	Stabilized	Routine	
0.31 – 0.39	10.65 – 12.59	11.00 – 12.00	Open midrise	
6	Acer pseudoplatanus			
Simple two-sided alignm.	Free	Stabilized	Routine	
0.29 – 0.35	4.50 – 6.10	11.00 – 12.00	Bare rock-paved	
7	Acer pseudoplatanus			
Grove	Free	Bare	Routine	
0.23 – 0.44	7.38 – 9.24	10.00 – 12.00	Compact midrise	
8	Platanus x acerifolia			
Isolated	Free	Stabilized	Routine	
0.41	16.66	10.00	Compact midrise	
9	Tilia x euchlora			
Grove	Free	Stabilized	Routine	
0.34 – 0.41	8.64 – 10.71	15.00 – 18.00	Compact midrise	
10	Fraxinus excelsior			
Simple one-sided alignm.	Free	Stabilized	Routine	
0.31 – 0.41	7.40 – 11.30	11.00 – 12.00	Water	
11	Platanus x acerifolia			
Grove	Free	Stabilized	Routine	
1.14 – 1.80	25.30 – 28.10	28.00 – 29.00	Compact midrise	
12	Acer pseudoplatanus			
Double one-sided alignm.	Free	Stabilized	Routine	
0.28 – 0.34	10.05 – 11.65	12.00 – 14.00	Bare rock-paved	
13	Tilia x euchlora			
Double central alignm.	Free	Grassed	Routine	
0.32 – 0.33	9.85 – 10.25	13.00 – 14.00	Bare rock-paved	
14	Platanus x acerifolia			
Isolated	Pruned	Bare	Routine	
1.13	20.10	25.00	Open lowrise	
15	Platanus x acerifolia			
Double central alignm.	Reconversion	Grassed	Routine	
0.51 – 0.52	11.01 – 11.92	15.00 – 16.00	Bare rock-paved	
16	Platanus x acerifolia			
Isolated	Free	Bare	Routine	
0.67	13.12	16.00	Open lowrise	
17	Platanus x acerifolia			
Double central alignm.	Pruned	Stabilized	Routine	
0.60 – 0.85	9.55 – 10.90	13.00 – 14.00	Open lowrise	
18	Platanus x acerifolia			
Simple one-sided alignm.	Free	Bare	Routine	
0.58 – 0.67	9.62 – 10.60	22.00 – 26.00	Open lowrise	
19	Platanus x acerifolia			
Double central alignm.	Pruned	Stabilized	Routine	
0.64 – 0.69	6.44 – 7.11	10.00 – 11.00	Bare rock-paved	

APPENDIX B

Changes in MSAVI2 values over 15-day windows

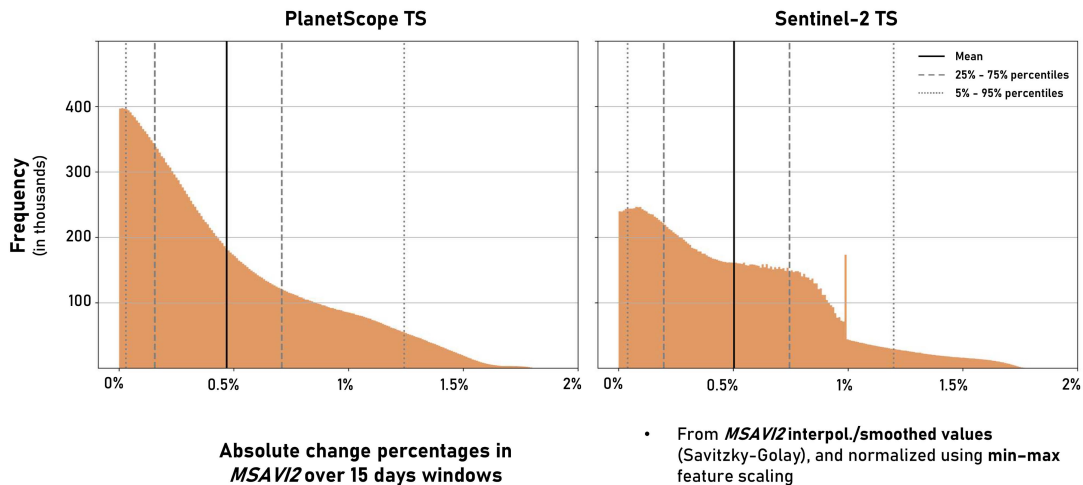
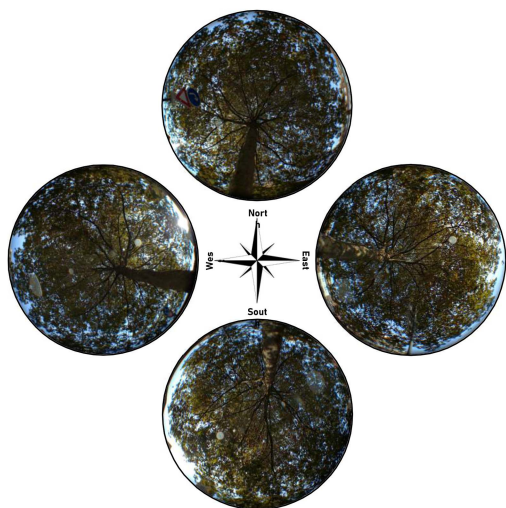


Fig. 9. Frequency of absolute percentage change in MSAVI2. These values are percentages of mean differences in consecutive values over 15-day windows, from interpolated, smoothed, and scaled S2 and PS data. Performed on 83 670 trees.

APPENDIX C

Examples of in situ acquisitions



Digital hemispherical photographs - LAI



Front-view digital photographs - GCC

Fig. 10. Example of DHP at each cardinal position around the same tree (left), and six front-view digital photographs taken during the year (right). Acquired on October 7, 2022—Site no. 8.

APPENDIX D

Spectral bands of S2 and PS sensors

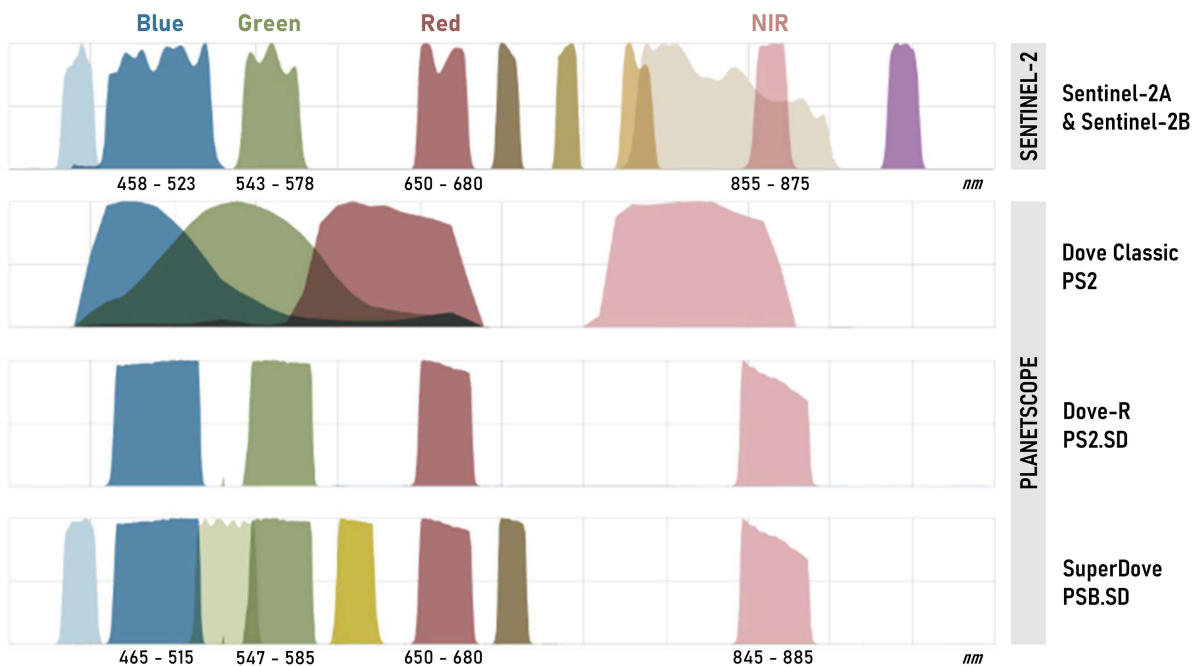


Fig. 11. Visualization of the spectral bands of S2 and PS sensors. The SuperDove harmonized bands and their wavelength ranges are displayed (adapted from [40]).



APPENDIX E

Comparison of *MSAVI2<sub>PS</sub>* and *MSAVI2<sub>S2</sub>* coregistered images

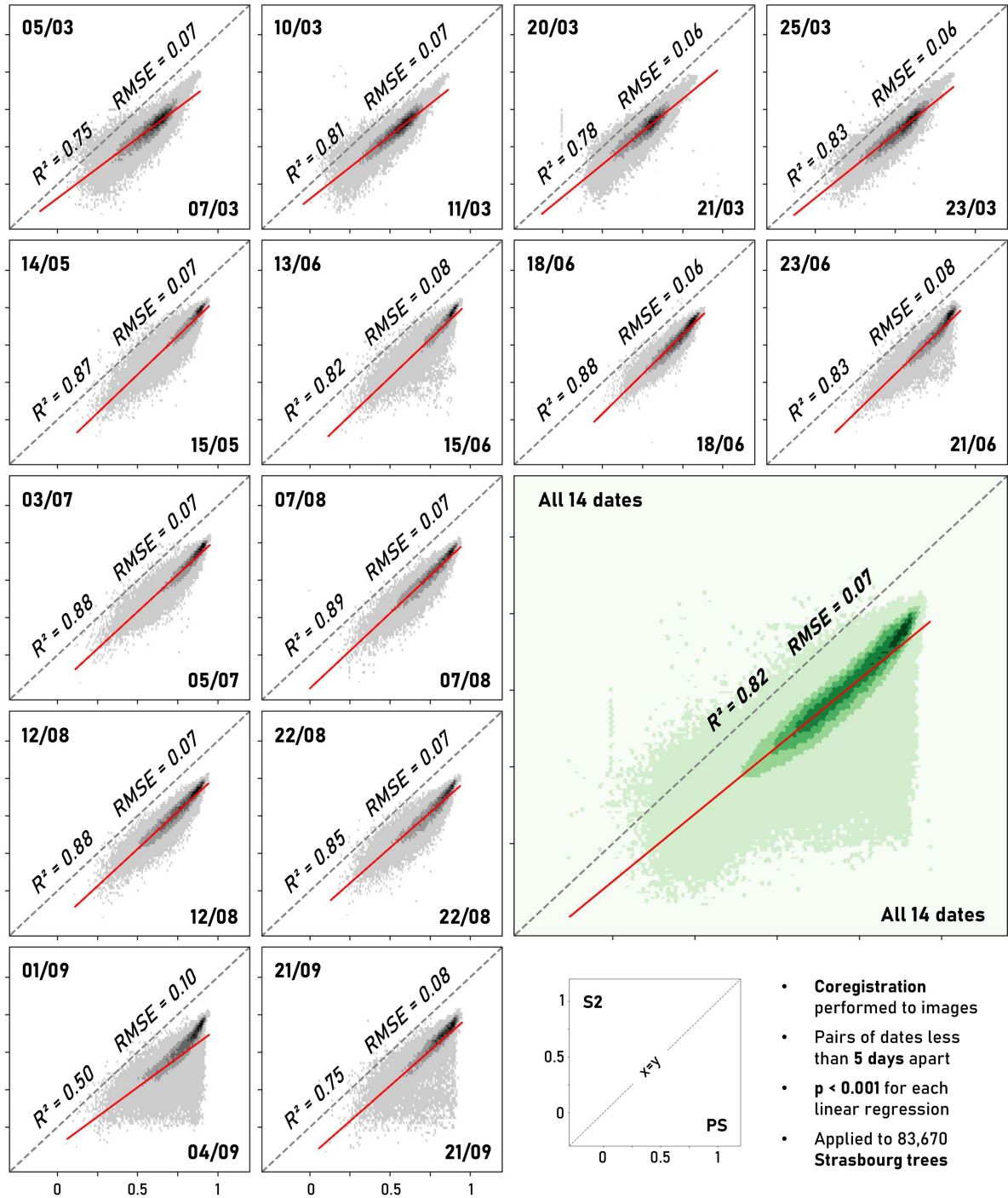


Fig. 12. Linear regressions of *MSAVI2* values for S2 and PS, for 14 pairs of coregistered close date (less than five days apart), and total. Performed on 83 670 trees.

## APPENDIX F

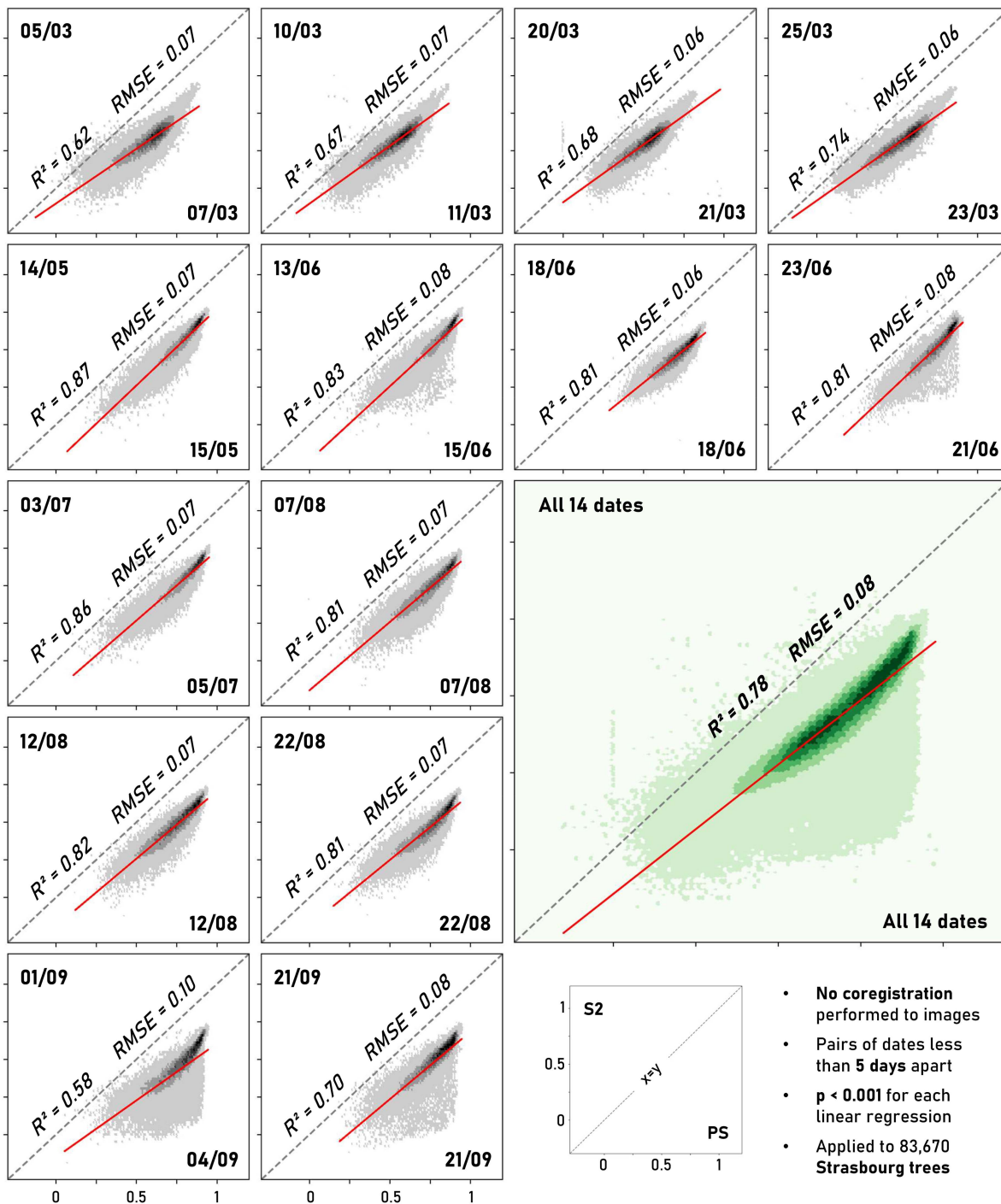
Comparison of *MSAVI2<sub>PS</sub>* and *MSAVI2<sub>S2</sub>* uncoregistered images

Fig. 13. Linear regressions of MSAVI2 values for S2 and PS, for 14 pairs of uncoregistered close date (less than five days apart), and total. Performed on 83 670 trees.

## ACKNOWLEDGMENT

The authors would like to thank the Strasbourg City Service (*Ville et Eurométropole de Strasbourg*) for providing the *Patrimoine arboré 2022* database. The authors would also like to thank M. Vermeil and R. Wenger (Laboratoire Image Ville Environnement, UMR 7362 CNRS, University of Strasbourg) for technical contributions.

## REFERENCES

- [1] F. Ferrini, C. C. K. Van den Bosch, and A. Fini, *Routledge Handbook of Urban Forestry*. New York, NY, USA: Taylor & Francis, 2017.
- [2] J. A. Salmond et al., "Health and climate related ecosystem services provided by street trees in the urban environment," *Environ. Health*, vol. 15, 2016, Art. no. S36.
- [3] P. Bolund and S. Hunhammar, "Ecosystem services in urban areas," *Ecol. Econ.*, vol. 29, pp. 293–301, 1999.
- [4] Y. Wang and H. Akbari, "The effects of street tree planting on urban heat island mitigation in Montreal," *Sustain. Cities Soc.*, vol. 27, pp. 122–128, 2016.
- [5] K. Zabret and M. Šraj, "Rainfall interception by urban trees and their impact on potential surface runoff," *CLEAN—Soil, Air, Water*, vol. 47, 2019, Art. no. 1800327.
- [6] S. Fares, E. Paoletti, C. Calfapietra, T. N. Mikkelsen, R. Samson, and D. L. Thiec, "Carbon sequestration by urban trees," in *The Urban Forest*. Cham, Switzerland: Springer, 2017, pp. 31–39.
- [7] E. Horváthová, T. Badura, and H. Duchková, "The value of the shading function of urban trees: A replacement cost approach," *Urban Forestry Urban Greening*, vol. 62, 2021, Art. no. 127166.
- [8] A. A. El-Khatib, N. A. Barakat, N. A. Youssef, and N. A. Samir, "Bioaccumulation of heavy metals air pollutants by urban trees," *Int. J. Phytoremediation*, vol. 22, pp. 210–222, 2020.
- [9] S. Stroud, J. Peacock, and C. Hassall, "Vegetation-based ecosystem service delivery in urban landscapes: A systematic review," *Basic Appl. Ecol.*, vol. 61, pp. 82–101, 2022.
- [10] G. Garland et al., "A closer look at the functions behind ecosystem multifunctionality: A review," *J. Ecol.*, vol. 109, no. 2, pp. 600–613, 2021.
- [11] R. Samson et al., "Urban trees and their relation to air pollution," in *The Urban Forest: Cultivating Green Infrastructure for People and the Environment*. Cham, Switzerland: Springer, 2017, pp. 21–30.
- [12] K. L. Hand, H. Rix, J. Stokes, and K. J. Doick, "The creation, content and use of urban tree strategies by English Local Governments," *Arboricultural J.*, vol. 44, pp. 183–207, 2022.
- [13] European Commission, "Communication from the commission to the European parliament, the Council, the European Economic and Social Committee and the committee of the regions New EU Forest Strategy for 2030," 2021. [Online]. Available: <https://eur-lex.europa.eu/legal-content/EN/TXT/?uri=CELEX%3A52021DC0572>
- [14] H. Pretzsch, A. Moser-Reischl, M. A. Rahman, S. Pauleit, and T. Rötzer, "Towards sustainable management of the stock and ecosystem services of urban trees. From theory to model and application," *Trees*, vol. 37, pp. 177–196, 2023.
- [15] P. Przewoźna, K. Maczka, M. Mielewczyk, A. Ingot, and P. Matczak, "Ranking ecosystem services delivered by trees in urban and rural areas," *Ambio*, vol. 51, pp. 2043–2057, 2022.
- [16] D. R. Hilbert, L. A. Roman, A. K. Koeser, J. Vogt, and N. S. Van Doorn, "Urban tree mortality: A literature review," *Arboriculture Urban Forestry*, vol. 45, no. 5, pp. 167–200, 2019.
- [17] D. S. L. Roux, K. Ikin, D. B. Lindenmayer, A. D. Manning, and P. Gibbons, "The future of large old trees in urban landscapes," *PLoS One*, vol. 9, no. 6, 2014, Art. no. e99403.
- [18] Z. Su et al., "Danger tree detection and tree number estimation based on UAV LiDAR data," *J. Univ. Chin. Acad. Sci.*, vol. 37, no. 6, pp. 760–766, 2020.
- [19] D. B. Lindenmayer and W. F. Laurance, "The ecology, distribution, conservation and management of large old trees," *Biol. Rev.*, vol. 92, no. 3, pp. 1434–1458, 2017.
- [20] G. Matasci, N. C. Coops, D. A. Williams, and N. Page, "Mapping tree canopies in urban environments using airborne laser scanning (ALS): A Vancouver case study," *Forest Ecosyst.*, vol. 5, pp. 1–9, 2018.
- [21] A. K. Ettinger, D. M. Buonaiuto, C. J. Chamberlain, I. Morales-Castilla, and E. M. Wolkovich, "Spatial and temporal shifts in photoperiod with climate change," *New Phytologist*, vol. 230, pp. 462–474, 2021.
- [22] T. Rötzer, A. Moser-Reischl, M. A. Rahman, R. Grote, S. Pauleit, and H. Pretzsch, "Modelling urban tree growth and ecosystem services: Review and perspectives," in *Progress in Botany*. Cham, Switzerland: Springer, 2020, pp. 405–464.
- [23] Y. Zhou, "Understanding urban plant phenology for sustainable cities and planet," *Nature Climate Change*, vol. 12, pp. 302–304, 2022.
- [24] J. Tang et al., "Emerging opportunities and challenges in phenology: A review," *Ecosphere*, vol. 7, 2016, Art. no. e01436.
- [25] S. Schnell, C. Kleinn, and G. Ståhl, "Monitoring trees outside forests: A review," *Environ. Monit. Assessment*, vol. 187, 2015, Art. no. 600.
- [26] U. Meier et al., "The BBCH system to coding the phenological growth stages of plants—History and publications," *J. für Kulturpflanzen*, vol. 61, no. 2, pp. 41–52, 2009.
- [27] H. Ressler, H. Scheifinger, T. Hübner, A. Paul, and M. Ungersböck, "PEP725: A European phenological database," in *Proc. EGU Gen. Assem. Conf. Abstr.*, 2021, Art. no. EGU21-2179.
- [28] M. Bonhomme, "Suivez le rythme avec TEMPO, le dernier né des SOER!," *J. du Centre INRA ARA*, vol. 2, 2017, Art. no. 6.
- [29] A. Donnelly et al., "Exploring discrepancies between in situ phenology and remotely derived phenometrics at NEON sites," *Ecosphere*, vol. 13, 2022, Art. no. e3912.
- [30] R. Neyens and F. Canters, "Mapping of urban vegetation with high-resolution remote sensing: A review," *Remote Sens.*, vol. 14, 2022, Art. no. 1031.
- [31] A. R. Shahtahmassebi et al., "Remote sensing of urban green spaces: A review," *Urban Forestry Urban Greening*, vol. 57, 2021, Art. no. 126946.
- [32] J. Xue and B. Su, "Significant remote sensing vegetation indices: A review of developments and applications," *J. Sens.*, vol. 2017, 2017, Art. no. 1353691.
- [33] J. Qi, Y. Kerr, and A. Chehbouni, "External factor consideration in vegetation index development," in *Proc. Int. Phys. Meas. Signatures Remote Sens.*, 1994, pp. 723–730.
- [34] C. Granero-Belinchon, K. Adeline, and X. Briottet, "Impact of the number of dates and their sampling on a NDVI time series reconstruction methodology to monitor urban trees with Ven  $\mu$  s satellite," *Int. J. Appl. Earth Observ. Geoinf.*, vol. 95, 2021, Art. no. 102257.
- [35] M. Löw and T. Koukal, "Phenology modelling and forest disturbance mapping with Sentinel-2 time series in Austria," *Remote Sens.*, vol. 12, 2020, Art. no. 4191.
- [36] P. J. Gómez-Giráldez, M. J. Pérez-Palazón, M. J. Polo, and M. P. González-Dugo, "Monitoring grass phenology and hydrological dynamics of an Oak–Grass Savanna ecosystem using Sentinel-2 and terrestrial photography," *Remote Sens.*, vol. 12, 2020, Art. no. 600.
- [37] M. Linkosalmi et al., "Tracking vegetation phenology of Pristine Northern Boreal Peatlands by combining digital photography with CO<sub>2</sub> flux and remote sensing data," *Biogeosciences*, vol. 19, pp. 4747–4765, 2022.
- [38] X. Chen, D. Wang, J. Chen, C. Wang, and M. Shen, "The mixed pixel effect in land surface phenology: A simulation study," *Remote Sens. Environ.*, vol. 211, pp. 338–344, 2018.
- [39] Y.-H. Tu, K. Johansen, B. Aragon, M. M. E. Hajj, and M. F. McCabe, "The radiometric accuracy of the 8-band multi-spectral surface reflectance from the planet superdove constellation," *Int. J. Appl. Earth Observ. Geoinf.*, vol. 114, 2022, Art. no. 103035.
- [40] T. Harrison and J. Mascaró, "Access to planet high spatial and temporal resolution Earth observation imagery via the NASA commercial SmallSat data acquisition (CSDA) program," in *Proc. 5th Planet. Data Workshop Planet. Sci. Inform. Analytics*, 2021, Art. no. 7107.
- [41] M. Gašparović, D. Dobričić, and I. Pilaš, "Mapping of allergenic tree species in highly urbanized area using PlanetScope imagery—A case study of Zagreb, Croatia," *Forests*, vol. 14, 2023, Art. no. 1193.
- [42] B. E. Lefulebe, A. V. Der Walt, and S. Xulu, "Fine-scale classification of urban land use and land cover with PlanetScope imagery and machine learning strategies in the city of Cape Town, South Africa," *Sustainability*, vol. 14, 2022, Art. no. 9139.
- [43] M. Alonzo, M. E. Baker, J. S. Caplan, A. Williams, and A. J. Elmore, "Canopy composition drives variability in urban growing season length more than the heat island effect," *Sci. Total Environ.*, vol. 884, 2023, Art. no. 163818.
- [44] M. Moon, A. D. Richardson, and M. A. Friedl, "Multiscale assessment of land surface phenology from harmonized Landsat 8 and Sentinel-2, PlanetScope, and Phenocam imagery," *Remote Sens. Environ.*, vol. 266, Dec. 2021, Art. no. 112716.

- [45] D. Browning, J. Karl, D. Morin, A. Richardson, and C. Tweedie, "Phenocams bridge the gap between field and satellite observations in an Arid Grassland ecosystem," *Remote Sens.*, vol. 9, 2017, Art. no. 1071.
- [46] A. D. Richardson et al., "Tracking vegetation phenology across diverse North American biomes using Phenocam imagery," *Sci. Data*, vol. 5, 2018, Art. no. 180028.
- [47] M. Pause et al., "In situ/remote sensing integration to assess forest health—A review," *Remote Sens.*, vol. 8, 2016, Art. no. 471.
- [48] J. Kim, Y. Ryu, C. Jiang, and Y. Hwang, "Continuous observation of vegetation canopy dynamics using an integrated low-cost, near-surface remote sensing system," *Agricultural Forest Meteorol.*, vol. 264, pp. 164–177, 2019.
- [49] V. Blanco, N. Willsea, T. Campbell, O. Howe, and L. Kalcsits, "Combining thermal imaging and soil water content sensors to assess tree water status in pear trees," *Front. Plant Sci.*, vol. 14, 2023, Art. no. 1197437.
- [50] C. J. Watson, N. Restrepo-Coupe, and A. R. Huete, "Multi-scale phenology of temperate grasslands: Improving monitoring and management with near-surface phenocams," *Front. Environ. Sci.*, vol. 7, 2019, Art. no. 14.
- [51] K. H. Tran, X. Zhang, A. R. Ketchpaw, J. Wang, Y. Ye, and Y. Shen, "A novel algorithm for the generation of gap-free time series by fusing harmonized Landsat 8 and Sentinel-2 observations with Phenocam time series for detecting land surface phenology," *Remote Sens. Environ.*, vol. 282, 2022, Art. no. 113275.
- [52] D. Yan, R. Scott, D. Moore, J. Biederman, and W. Smith, "Understanding the relationship between vegetation greenness and productivity across dryland ecosystems through the integration of Phenocam, satellite, and eddy covariance data," *Remote Sens. Environ.*, vol. 223, pp. 50–62, 2019.
- [53] G. Filippa et al., "Phenopix: A R package for image-based vegetation phenology," *Agricultural Forest Meteorol.*, vol. 220, pp. 141–150, 2016.
- [54] M. Girondot, "phenology: Tools to manage a parametric function that describes phenology and more," 2019. [Online]. Available: <https://cran.r-project.org/web/packages/phenology/index.html>
- [55] P. Jönsson and L. Eklundh, "TimeSat—A program for analyzing time-series of satellite sensor data," *Comput. Geosci.*, vol. 30, pp. 833–845, 2004.
- [56] M. Forkel and T. Wutzler, "Greenbrown—Land surface phenology and trend analysis," A Package for the R Software, Version 2.2, 2015. [Online]. Available: <http://greenbrown.r-forge.r-project.org/>
- [57] K. Hufkens et al., "Monitoring crop phenology using a smartphone based near-surface remote sensing approach," *Agricultural Forest Meteorol.*, vol. 265, pp. 327–337, 2019.
- [58] R. Casa, D. Upreti, and F. Pelosi, "Measurement and estimation of leaf area index (LAI) using commercial instruments and smartphone-based systems," *IOP Conf. Ser.: Earth Environ. Sci.*, vol. 275, 2019, Art. no. 012006.
- [59] M. Campos-Taberner et al., "Use of smartphones as measuring tools for educational purposes in remote sensing," in *Proc. 11th Int. Technol., Educ. Develop. Conf.*, 2017, pp. 5474–5478.
- [60] *Fiche Climatologique: Statistiques 1991–2020 et Records (in French)*, Météo France, Toulouse, France, 2023. [Online]. Available: [https://donneespubliques.meteofrance.fr/FichesClim/FICHECLIM\\_67124001.pdf](https://donneespubliques.meteofrance.fr/FichesClim/FICHECLIM_67124001.pdf)
- [61] *Plan canopée: La végétalisation de la ville par l'arbre urbain*, Ville et Eurométropole de Strasbourg, Strasbourg, France, 2020. [Online]. Available: <https://www.strasbourg.eu/documents/976405/1628244/07aa73854-7e07-ad0b-7655-33d8c08cc636>
- [62] *Patrimoine arboré*, Ville et Eurométropole de Strasbourg, Strasbourg, France, 2022. [Online]. Available: [https://data.strasbourg.eu/explore/dataset/patrimoine\\_arbore/](https://data.strasbourg.eu/explore/dataset/patrimoine_arbore/)
- [63] M. Persson, E. Lindberg, and H. Reese, "Tree species classification with multi-temporal Sentinel-2 data," *Remote Sens.*, vol. 10, 2018, Art. no. 1794.
- [64] M. Rautiainen, P. Stenberg, T. Nilson, and A. Kuusk, "The effect of crown shape on the reflectance of coniferous stands," *Remote Sens. Environ.*, vol. 89, pp. 41–52, 2004.
- [65] E. Prudnikova, I. Savin, G. Vindeker, P. Grubina, E. Shishkonakova, and D. Sharychev, "Influence of soil background on spectral reflectance of winter wheat crop canopy," *Remote Sens.*, vol. 11, 2019, Art. no. 1932.
- [66] K. Johansen, T. Raharjo, and M. McCabe, "Using multi-spectral UAV imagery to extract tree crop structural properties and assess pruning effects," *Remote Sens.*, vol. 10, 2018, Art. no. 854.
- [67] I. D. Stewart and T. R. Oke, "Local climate zones for urban temperature studies," *Bull. Amer. Meteorol. Soc.*, vol. 93, pp. 1879–1900, 2012.
- [68] D. Helman, "Land surface phenology: What do we really 'see' from space?," *Sci. Total Environ.*, vol. 618, pp. 665–673, 2018.
- [69] P. Balakrishnan and J. A. Jakubiec, "Trees in daylight simulation—Measuring and modelling realistic light transmittance through trees," *LEUKOS*, vol. 19, pp. 241–268, 2023.
- [70] T. Taghavi, A. Rahemi, and E. Suarez, "Development of a uniform phenology scale (BBCH) in Hazelnuts," *Scientia Horticulturae*, vol. 296, 2022, Art. no. 110837.
- [71] G. Finn, A. Straszewski, and V. Peterson, "A general growth stage key for describing trees and woody plants," *Ann. Appl. Biol.*, vol. 151, no. 1, pp. 127–131, 2007.
- [72] G. M. Díaz and J. D. Lencinas, "Model-based local thresholding for canopy hemispherical photography," *Can. J. Forest Res.*, vol. 48, pp. 1204–1216, 2018.
- [73] K. L. Beeles, J. C. Tourville, and M. Dovciak, "Characterizing canopy openness across large forested landscapes using spherical densiometer and smartphone hemispherical photography," *J. Forestry*, vol. 120, pp. 37–50, 2022.
- [74] J. Konarska, J. Klingberg, and F. Lindberg, "Applications of dual-wavelength hemispherical photography in urban climatology and urban forestry," *Urban Forestry Urban Greening*, vol. 58, 2021, Art. no. 126964.
- [75] A. Brusa and D. E. Bunker, "Increasing the precision of canopy closure estimates from hemispherical photography: Blue channel analysis and under-exposure," *Agricultural Forest Meteorol.*, vol. 195/196, pp. 102–107, 2014.
- [76] S. Paramanik, M. Behera, and J. Dash, "Symbolic regression-based allometric model development of a mangrove forest LAI using structural variables and digital hemispherical photography," *Appl. Geography*, vol. 139, 2022, Art. no. 102649.
- [77] I. G. C. Jonckheere, C. Macfarlane, and J.-M. N. Walter, "Image analysis of hemispherical photographs, algorithms and calculations," in *Hemispherical Photography in Forest Science: Theory, Methods, Applications*. Dordrecht, The Netherlands: Springer, 2017, pp. 115–151.
- [78] F. Chianucci and M. Macek, "hemispher: An R package for fisheye canopy image analysis," *Agricultural Forest Meteorol.*, vol. 336, 2023, Art. no. 109470.
- [79] N. Otsu, "A threshold selection method from gray-level histogram," *IEEE Trans. Syst., Man, Cybern.*, vol. 9, no. 1, pp. 62–66, Jan. 1979.
- [80] M. Grotti et al., "An intensity, image-based method to estimate gap fraction, canopy openness and effective leaf area index from phase-shift terrestrial laser scanning," *Agricultural Forest Meteorol.*, vol. 280, 2020, Art. no. 107766.
- [81] M. Nobis and U. Hunziker, "Automatic thresholding for hemispherical canopy-photographs based on edge detection," *Agricultural Forest Meteorol.*, vol. 128, nos. 3/4, pp. 243–250, 2005.
- [82] J. Zou et al., "Evaluating the impact of sampling schemes on leaf area index measurements from digital hemispherical photography in Larix principis-rupprechtii forest plots," *Forest Ecosyst.*, vol. 7, pp. 1–18, 2020.
- [83] P. J. Peper and E. G. McPherson, "Evaluation of four methods for estimating leaf area of isolated trees," *Urban Forestry Urban Greening*, vol. 2, no. 1, pp. 19–29, 2003.
- [84] Z. Liu et al., "Fractional coverage rather than green chromatic coordinate is a robust indicator to track grassland phenology using smartphone photography," *Ecol. Inform.*, vol. 68, 2022, Art. no. 101544.
- [85] Z. Liu, S. An, X. Lu, H. Hu, and J. Tang, "Using canopy greenness index to identify leaf ecophysiological traits during the Foliar senescence in an Oak Forest," *Ecosphere*, vol. 9, 2018, Art. no. e02337.
- [86] Y. Luo et al., "Potential and limitations of using digital repeat photography to track structural and physiological phenology in Mediterranean tree-grass ecosystems," in *Proc. EGU Gen. Assem. Conf. Abstr.*, 2017, Art. no. 8660.
- [87] F. Liu, X. Wang, and C. Wang, "Measuring vegetation phenology with near-surface remote sensing in a temperate deciduous forest: Effects of sensor type and deployment," *Remote Sens.*, vol. 11, 2019, Art. no. 1063.
- [88] A. Stumpf, D. Michéa, and J.-P. Malet, "Improved co-registration of Sentinel-2 and Landsat-8 imagery for Earth surface motion measurements," *Remote Sens.*, vol. 10, 2018, Art. no. 160.
- [89] A. J. Richardson and C. Wiegand, "Distinguishing vegetation from soil background information," *Photogrammetric Eng. Remote Sens.*, vol. 43, no. 12, pp. 1541–1552, 1977.
- [90] J. Qi, A. Chehbouni, A. Huete, Y. Kerr, and S. Sorooshian, "A modified soil adjusted vegetation index," *Remote Sens. Environ.*, vol. 48, pp. 119–126, 1994.

- [91] A. Bhatt, S. K. Ghosh, and A. Kumar, "Spectral indices based change detection in an urban area using Landsat data," in *Proc. 5th Int. Conf. Soft Comput. Probl. Solving*, 2016, pp. 425–441.
- [92] E. Arafat and I. M. Rafizul, "Remote sensing techniques as a tool for environmental monitoring in and around of Rajbandh Landfill at Khulna City," *J. Eng. Sci.*, vol. 13, pp. 127–137, 2023.
- [93] D. Scheffler, A. Hollstein, H. Diedrich, K. Segl, and P. Hostert, "AROSICS: An automated and robust open-source image co-registration software for multi-sensor satellite data," *Remote Sens.*, vol. 9, 2017, Art. no. 676.
- [94] S. Jabari and Y. Zhang, "RPC-based coregistration of VHR imagery for urban change detection," *Photogrammetric Eng. Remote Sens.*, vol. 82, no. 7, pp. 521–534, 2016.
- [95] A. Savitzky and M. J. E. Golay, "Smoothing and differentiation of data by simplified least squares procedures," *Anal. Chem.*, vol. 36, pp. 1627–1639, 1964.
- [96] J. Chen, P. Jönsson, M. Tamura, Z. Gu, B. Matsushita, and L. Eklundh, "A simple method for reconstructing a high-quality NDVI time-series data set based on the Savitzky–Golay filter," *Remote Sens. Environ.*, vol. 91, pp. 332–344, 2004.
- [97] A. Bachoo and S. Archibald, "Influence of using date-specific values when extracting phenological metrics from 8-day composite NDVI data," in *Proc. Int. Workshop Anal. Multi-Temporal Remote Sens. Images*, 2007, pp. 1–4.
- [98] H. Han, J. Bai, G. Ma, and J. Yan, "Vegetation phenological changes in multiple landforms and responses to climate change," *ISPRS Int. J. Geo-Inf.*, vol. 9, no. 2, 2020, Art. no. 111.
- [99] J. A. Caparros-Santiago, V. Rodriguez-Galiano, and J. Dash, "Land surface phenology as indicator of global terrestrial ecosystem dynamics: A systematic review," *ISPRS J. Photogrammetry Remote Sens.*, vol. 171, pp. 330–347, 2021.
- [100] D. G. Brown and J.-D. Duh, "Spatial simulation for translating from land use to land cover," *Int. J. Geographical Inf. Sci.*, vol. 18, pp. 35–60, 2004.
- [101] S. Openshaw, M. Charlton, and S. Carver, "Error propagation: A Monte Carlo simulation," in *Handling Geographical Information: Methodology and Potential Applications*, I. Masser and M. Blakemore Eds., New York, NY, USA: Wiley, 1991, pp. 102–114.
- [102] D. G. Hadjimitsis, C. Clayton, and L. Toullos, "Retrieving visibility values using satellite remote sensing data," *Phys. Chem. Earth, A/B/C*, vol. 35, pp. 121–124, 2010.
- [103] S. C. Goslee, "Analyzing remote sensing data in R: The Landsat package," *J. Statist. Softw.*, vol. 43, pp. 1–25, 2011.
- [104] T. Jautzy, P.-A. Herrault, V. Chardon, L. Schmitt, and G. Rixhon, "Measuring river planform changes from remotely sensed data—A Monte Carlo approach to assessing the impact of spatially variable error," *Earth Surf. Dyn.*, vol. 8, pp. 471–484, 2020.
- [105] C. Granero-Belinchon, K. Adeline, A. Lemonsu, and X. Briotet, "Phenological dynamics characterization of alignment trees with Sentinel-2 imagery: A vegetation indices time series reconstruction methodology adapted to urban areas," *Remote Sens.*, vol. 12, 2020, Art. no. 639.
- [106] E. K. Melaas, J. A. Wang, D. L. Miller, and M. A. Friedl, "Interactions between urban vegetation and surface urban heat islands: A case study in the Boston Metropolitan Region," *Environ. Res. Lett.*, vol. 11, 2016, Art. no. 054020.
- [107] X. Zhang, M. A. Friedl, C. B. Schaaf, A. H. Strahler, and A. Schneider, "The footprint of urban climates on vegetation phenology," *Geophys. Res. Lett.*, vol. 31, 2004, Art. no. L12209.
- [108] M. Zhu et al., "Mapping 24 woody plant species phenology and ground forests phenology over China from 1951–2020," *Earth Syst. Sci. Data Discuss.*, vol. 2023, pp. 1–26, 2023.
- [109] Y. Zhao et al., "Evaluating fine-scale phenology from PlanetScope satellites with ground observations across temperate forests in Eastern North America," *Remote Sens. Environ.*, vol. 283, 2022, Art. no. 113310.
- [110] D. S. Park, E. A. Newman, and I. K. Breckheimer, "Scale gaps in landscape phenology: Challenges and opportunities," *Trends Ecol. Evol.*, vol. 36, pp. 709–721, 2021.
- [111] V. P. Nolan and J. F. Weltzin, "Phenology for science, resource management, decision making, and education," *Eos, Trans. Amer. Geophys. Union*, vol. 92, p. 15, 2011.
- [112] L. Zeng, B. D. Wardlow, D. Xiang, S. Hu, and D. Li, "A review of vegetation phenological metrics extraction using time-series, multispectral satellite data," *Remote Sens. Environ.*, vol. 237, 2020, Art. no.111511.
- [113] H. Huang and D. Roy, "Characterization of PlanetScope-0 PlanetScope-1 surface reflectance and normalized difference vegetation index continuity," *Sci. Remote Sens.*, vol. 3, 2021, Art. no. 100014.
- [114] M. Moon, A. D. Richardson, T. Milliman, and M. A. Friedl, "A high spatial resolution land surface phenology dataset for AmeriFlux and neon sites," *Sci. Data*, vol. 9, 2022, Art. no.448.
- [115] K. Bórnez, A. Descals, A. Verger, and J. Peñuelas, "Land surface phenology from VEGETATION and PROBA-V data. Assessment over deciduous forests," *Int. J. Appl. Earth Observ. Geoinf.*, vol. 84, 2020, Art. no. 101974.
- [116] T. F. Keenan et al., "Tracking forest phenology and seasonal physiology using digital repeat photography: A critical assessment," *Ecol. Appl.*, vol. 24, pp. 1478–1489, 2014.
- [117] A. Donnelly and R. Yu, "The rise of phenology with climate change: An evaluation of IJB publications," *Int. J. Biometeorol.*, vol. 61, pp. 29–50, 2017.
- [118] Q. Xin, J. Li, Z. Li, Y. Li, and X. Zhou, "Evaluations and comparisons of rule-based and machine-learning-based methods to retrieve satellite-based vegetation phenology using MODIS and USA national phenology network data," *Int. J. Appl. Earth Observ. Geoinf.*, vol. 93, 2020, Art. no. 102189.
- [119] K. F. Huemrich, S. V. Zesati, P. Campbell, and C. Tweedie, "Canopy reflectance models illustrate varying NDVI responses to change in high latitude ecosystems," *Ecol. Appl.*, vol. 31, 2021, Art. no. e02435.
- [120] D. Richards and J. W. Wang, "Fusing street level photographs and satellite remote sensing to map leaf area index," *Ecol. Indicators*, vol. 115, 2020, Art. no. 106342.
- [121] Y. Vitasse, A. J. Porté, A. Kremer, R. Michalet, and S. Delzon, "Responses of canopy duration to temperature changes in four temperate tree species: Relative contributions of spring and autumn leaf phenology," *Oecologia*, vol. 161, pp. 187–198, 2009.
- [122] Y. Zhao and D. Liu, "A robust and adaptive spatial-spectral fusion model for PlanetScope and Sentinel-2 imagery," *GISci. Remote Sens.*, vol. 59, pp. 520–546, 2022.
- [123] M. Gašparović, D. Medak, I. Pilaš, L. Jurjević, and I. Balenović, "Fusion of Sentinel-2 and PlanetScope imagery for vegetation detection and monitoring," *Int. Arch. Photogrammetry, Remote Sens. Spatial Inf. Sci.*, vol. XLII-1, pp. 155–160, 2018.
- [124] Y. Sadeh et al., "Fusion of Sentinel-2 and PlanetScope time-series data into daily 3 m surface reflectance and wheat LAI monitoring," *Int. J. Appl. Earth Observ. Geoinf.*, vol. 96, 2021, Art. no. 102260.
- [125] K. F. Battle et al., "Citizen science across two centuries reveals phenological change among plant species and functional groups in the Northeastern US," *J. Ecol.*, vol. 110, pp. 1757–1774, 2022.
- [126] I. Dronova and S. Taddeo, "Remote sensing of phenology: Towards the comprehensive indicators of plant community dynamics from species to regional scales," *J. Ecol.*, vol. 110, pp. 1460–1484, 2022.
- [127] X. Wu, Q. Xiao, J. Wen, D. You, and A. Hueni, "Advances in quantitative remote sensing product validation: Overview and current status," *Earth-Sci. Rev.*, vol. 196, 2019, Art. no. 102875.
- [128] A. Baccini, M. Friedl, C. Woodcock, and Z. Zhu, "Scaling field data to calibrate and validate moderate spatial resolution remote sensing models," *Photogrammetric Eng. Remote Sens.*, vol. 73, no. 8, pp. 945–954, 2007.
- [129] L. Eklundh, H. Jin, P. Schubert, R. Guzinski, and M. Heliasz, "An optical sensor network for vegetation phenology monitoring and satellite data calibration," *Sensors*, vol. 11, no. 8, pp. 7678–7709, 2011.
- [130] N. Restrepo-Coupe, A. Huete, and K. Davies, "Satellite phenology validation," in *AusCover Good Practice Guidelines: A Technical Handbook Supporting Calibration and Validation Activities of Remotely Sensed Data Product*. Indooroopilly, QLD, Australia: TERN AusCover, 2015, pp. 155–157.
- [131] F. Tian et al., "Calibrating vegetation phenology from Sentinel-2 using eddy covariance, PhenoCam, and PEP725 networks across Europe," *Remote Sens. Environ.*, vol. 260, 2021, Art. no. 112456.
- [132] S. Piao et al., "Plant phenology and global climate change: Current progresses and challenges," *Glob. Change Biol.*, vol. 25, no. 6, pp. 1922–1940, 2019.
- [133] J. L. Araus and S. C. Kefauver, "Breeding to adapt agriculture to climate change: Affordable phenotyping solutions," *Curr. Opin. Plant Biol.*, vol. 45, pp. 237–247, 2018.
- [134] J. Klingberg, J. Konarska, F. Lindberg, L. Johansson, and S. Thorsson, "Mapping leaf area of urban greenery using aerial LiDAR and ground-based measurements in Gothenburg, Sweden," *Urban Forestry Urban Greening*, vol. 26, pp. 31–40, 2017.

- [135] S. Wei et al., "An assessment study of three indirect methods for estimating leaf area density and leaf area index of individual trees," *Agricultural Forest Meteorol.*, vol. 292, 2020, Art. no. 108101.
- [136] D. M. Jaeger, A. Looze, M. Raleigh, B. W. Miller, J. Friedman, and C. Wessman, "From flowering to foliage: Accelerometers track tree sway to provide high-resolution insights into tree phenology," *Agricultural Forest Meteorol.*, vol. 318, 2022, Art. no. 108900.
- [137] O. Sonnentag et al., "Digital repeat photography for phenological research in forest ecosystems," *Agricultural Forest Meteorol.*, vol. 152, pp. 159–177, 2012.

**Clément Bressant** received the B.Sc. degree in geography and planning from the University of Bourgogne, Dijon, France, in 2019, and the M.Sc. degree in earth observation and geomatics in 2021 from the University of Strasbourg, Strasbourg, France, where he is currently working toward the Ph.D. degree.

His Ph.D. thesis focuses on hypertemporal remote sensing of urban tree vegetation, with a view to monitoring, managing, and estimating the contribution of trees to their environment.

**Pierre-Alexis Herrault** received the M.Sc. degree in geomatics from the University of Rennes, Rennes, France, in 2011, and the Ph.D. degree in geography from the University of Toulouse, Toulouse, France, in 2015.

His thesis focused on the reconstruction of forest changes to evaluate the effects of history on current biodiversity. From 2015 to 2017, he was a Post-doctoral Research Associate with the Centre d'Études Spatiales de la Biosphère Laboratory, Toulouse. Since 2017, he has been an Associate Professor with the Laboratoire Image Ville Environnement, University of Strasbourg, Strasbourg, France. His research interests include remote sensing for landscape ecology and estimating biodiversity, old spatial data processing, and uncertainty assessment in land cover changes from spatial data.

**Anne Puissant** received the Ph.D. degree in geography and remote sensing from the University of Strasbourg, Strasbourg, France, in 2003.

From 2004 to 2017, she was an Associate Professor with the University of Strasbourg, where she has been a Professor of Earth Observation and Geomatics since 2018. She is pursuing research tasks at the interface between geosciences and computer sciences with the development of image processing methods based on artificial intelligence. Since 2022, she has been the Head of the THEIA Data and Services Centre, part of the Research Infrastructure Data Terra, Montpellier, France. Her research interests include exploitation of earth observation images for assessing land cover/use dynamics at several spatial scales.